Evaluation of a semi-empirical numerical simulation method for level ice breaking

Fang Li

School of Engineering

Thesis submitted for examination for the degree of Master of Science in Technology.

Espoo 30.6.2016

Thesis supervisor:

Prof. Pentti Kujala

Prof. Sören Ehlers

Thesis advisor:

M.Sc. Lauri Kuuliala

Aalto University
School of Engineering

AALTO UNIVERSITY
SCHOOL OF ENGINEERING

ABSTRACT OF THE
MASTER'S THESIS

Author: Fang Li

Title: Evaluation of a semi-empirical numerical simulation method for level ice breaking

Date: 30.6.2016 Language: English Number of pages: 6+66

Department of Mechanical Engineering

Professorship: Maritime Engineering

Supervisor: Prof. Pentti Kujala & Prof. Sören Ehlers

Advisor: M.Sc. Lauri Kuuliala

A semi-empirical numerical method for level ice breaking is evaluated in this thesis by full scale data from ice trial of S.A. Agulhas II. The data are analysed and organised systematically for evaluation use with certain accuracy. The original model together with some improved versions are evaluated in terms of ship resistance, time history of speed and average speed. Additional resistance source is identified. A comparison between empirical formulas and simulation methods is conducted to find the advantages and deficiencies of this method.

Results have shown that this model generally gives acceptable prediction on average resistance and velocity. However, there are obvious deviations in time history of velocity. Compared to empirical formulas, numerical method gives more ship-specific results. Besides, shoulder crushing is identified as an important phenomenon which introduces uncertainty in results. Randomness is suggested for ice breaking pattern to eliminate this problem.

As suggestion, a combined modification including dynamic bending and random breaking radius is recommended. Resistance due to ice rubble under level ice is required to be included in ship resistance. A combined ice thickness measurement including electromagnetic method and stereo camera is suggested to grasp more information of the ice. Model and full scale tests are required to investigate more about ice breaking process, especially breaking pattern. This model can be improved when some empirical coefficients are replaced by conclusions from test results.

Keywords: level ice, ice breaking, numerical simulation, breaking pattern

Preface

I want to thank Professor Pentti Kujala for giving me this opportunity to write my thesis at Marine Technology unit, Aalto University. During the six months' work, I learned a lot within Arctic technology. My research skill has improved a lot and I am now prepared for possible future research. Also I would like to give thanks to Professor Sören Ehlers, my second supervisor from NTNU, for giving me suggestions and feedback.

Besides, I am glad to thank my advisor, Lauri Kuuliala, for his instructions and guidance during the whole process. He helped me to keep moving on with a proper schedule and was always in time to give me advice and feedback. He also kept me working in the right direction and saved me lots of time from unnecessary work. I hope this thesis could be helpful for his own research.

I also received help from some doctoral students in the laboratory. Mikko Suominen provided me with the full scale data and gave me thorough instructions on that. Hanyang Gong made me realise the presence and importance of ridge resistance, which is a great push for my research progress.

In addition, I would like to thank my girlfriend, Haojie Ye, for being with me. Her support gives me motion to do the work better. Also I need to thank my parents in China who support me mentally and care about me all the time.

Otaniemi, 30.6.2016

Fang Li

Contents

Symbols

$\mathbf{A}$	Added mass matrix
A_c	Contact area
$\mathbf{B}$	Damping matrix
B	Ship breadth
$\mathbf{C}$	Hydrostatic restoring matrix
C_b	Volumetric block coefficient
C_l, C_v and C_f	Empirical coefficients of the ice-breaking model
E	Strain modulus
$\mathbf{F}$	Force vector
F_c	Crushing force
F_H	Horizontal force due to ice contact
F_V	Vertical force due to ice contact
f_H	Vertical frictional force due to ice contact
h_i	Ice thickness
h_r	Ice rubble thickness
I_{zz}	Moment of inertia about z-axis
L	Waterline length
L_{par}	Parallel ship body length
l_c	Characteristic length of ice
L_h and L_d	Contact length and indentation depth
$\mathbf{M}$	Mass matrix
m	Ship mass
P_f	Bearing capacity of an ice wedge
R	Breaking radius of ice
R_i, R_c, R_b, R_s and R_r	Total, crushing, breaking, submersion and ridge ice resistance
$\mathbf{x}$, $\dot{\mathbf{x}}$ and $\ddot{\mathbf{x}}$	Position, velocity and acceleration vector
T	Draught (in tables) or thrust (in figures)
T_b	Bollard pull
T_{net}	Net thrust
v_{ow}	Open water speed
v^{rel}	Relative velocity between hull and ice
v_t^{rel} and v_n^{rel}	Component of relative velocity tangential and normal to contact area
X, Y and Z	Coordinates in the global coordinate system
X_G and Y_G	Coordinates of the center of gravity of the ship
x, y and z	Coordinates in the ship coordinate system
α	Entrance waterline angle
μ	Friction coefficient
ν	Poisson's ratio
Ψ	Heading angle of the ship
ϕ	Flare angle at contact area
ρ_i and ρ_w	Density of ice and water
σ_c	Crushign strength
σ_f	Bending strength
θ	Opening angle of ice wedge

1 Introduction

1.1 Background

Today the melting of ice in the Arctic area has drawn the attention of many scientists and researchers. Significant effort has been put into reducing and preventing this environmental issue. However, despite of the environmental influence, this phenomenon is also making this area more accessible, which is seen as an opportunity by shipping, oil and gas companies. The length of route between Asia and America as well as Asia and Europe is greatly shortened via Arctic area, which means less fuel consumption, less passage time and more profit.

Figure 1 illustrating the respective monthly averages ice extent during the winter maximum and summer minimum extents. There have been several sailing routes transiting along the coastline of Russia and Canada in summer, where there is no multi-year ice covering. With the shrinking of ice covered area and the progress in Arctic technology, the trafficability of Arctic area is expected to increase further.

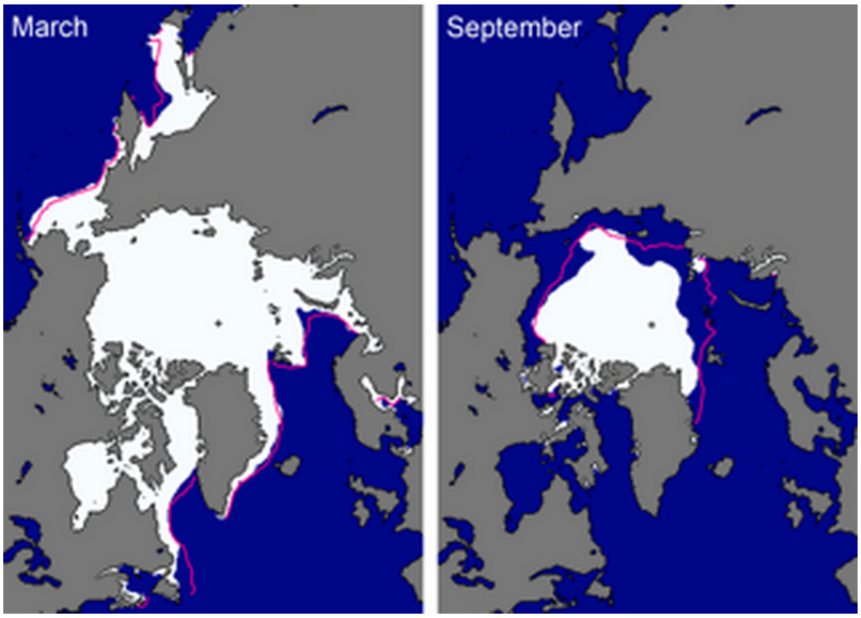

Figure 1: Sea ice extent in March 2013 (left) and September 2013 (right) (en.wikipedia.org/wiki/Arctic_shipping_routes)

Ice conditions can be very complex and diverse. It can be divided according to the stage of formation as well as shapes and features. Resistance formulas have been proposed by researchers on level ice (e.g. Lindqvist, 1989), ridged ice (e.g. Malmberg, 1983), channel ice (e.g. Riska et al., 1997) as well as other types of ice. Of all the ice conditions, level ice is mostly used as a criteria for the ice breaking capacity of ships, since it is relatively easy to model.

Icebreakers are designed and developed from an early age. Jones (2004) presented a historical review of the scientific literature on ship performance in ice. As mentioned there, icebreaker research can date back to 1888/89. From early 20th century, some

empirical formulas were developed to decide the power and dimension requirements for icebreaking. Then in late 20th century, empirical formulas regarding ice going resistance and ice breaking patterns (e.g. level ice resistance formula by Lindqvist (1989)) are proposed by researchers and put into use. Advances in ship-ice modelling techniques both experimental and numerical have been seen in last thirty years. (Jones 2004)

There are several forces occurring simultaneously during ship-ice interaction. Crushing and bending are regarded as two dominant forces during ice breaking by many researchers, while buoyancy and clearing forces are significant in underwater part. In some literature (e.g. Zhou, 2012), ice rubble accumulation is also concentrated on and simulated numerically. Since brittle failure is important during ice contacting (Timco & Weeks, 2010), the pressure shows a dependence on contact area, which affects loading process. This has been investigated by many researchers (e.g. Daley, 2007). All of these need to be considered in simulation.

1.2 Aims and scope of the thesis

This thesis involves a numerical simulation model proposed by Su (2011) for the use of prediction of ship motions, loads and resistance when it is breaking level ice in continuous mode. The model is validated using full scale data from ship trials by icebreaker S.A. Agulhas II. Some modifications are done to the model to see potential improvements in this model. The first one is a modification regarding ice bearing capacity according to Tan et al. (2014). The second is a non-linear pressure-area relationship within the contact area. The third one is a random floe radius model proposed in Su et al. (2014) and the last one is an area modification according to Zhou et al. (2016). These modifications are analysed in detail to find a potential way to improve the model. Besides, a ridge resistance formula by Riska et al. (1997) based on Malmberg (1983) is incorporated into the model to take account rubble resistance.

Generally, there are two main research questions: how good the model is for predicting level ice resistance, and what can be improved in this model for a better prediction. The author hopes that the readers can get a comprehensive understanding on the usability, advantages, deficiencies and possible improvements of the model. Thereby this thesis could act as an instruction for researchers who apply this model. Specifically, there are following points to be discussed

- Find an effective way to organise the data from full scale test for evaluation use.
- Evaluate the capability of Su's model for the use of predicting continuous motion of a ship under changing power and ice conditions.
- Compare the capacity of resistance prediction by Su's model to those by empirical formulas, especially Lindqvist's and Riska's formula.

- Implement a dynamic bending bearing capacity, a non-linear pressure-area relationship and a random breaking radius into the model and check if these improve the results.
- Discuss the influence of a contact area modification to the model.
- Identify other potential resistance source and incorporate that into the model.
- Give suggestions on the application of this model and propose possible improvements.

In chapter 2, a state of art study on level ice breaking simulation is conducted. Focus is on different numerical models proposed by researchers. In chapter 3, resistance prediction methods used in this thesis are described in detail. Two empirical formulas are introduced and the mechanism of numerical simulation model is explained. Then in chapter 4, a description and analysis of measurement methods onboard S.A. Agulhas II is conducted. Full scale data used for evaluation is described and preliminarily analysed. A qualitative discussion on ice breaking process and evaluation criteria is conducted in chapter 5. In chapter 6, the simulation process is introduced. Results of the simulation are presented in chapter 7. The discussion on the simulation results are conducted in chapter 8. Finally, conclusions and recommendations are given in chapter 9.

2 State of Art study of level ice breaking simulation methods

Ice breaking simulation has been developed by researchers for several decades. Empirical, analytical and numerical methods as well as other approaches are used to simulate ship-ice interaction. Since ice breaking mechanism is complex, it involves researches on various topics, such as pressure-area relationship and ice breaking pattern. In this chapter, the development of the simulation model used in this thesis is firstly introduced, followed by other simulation methods for ship-ice interaction. Then a brief study on current research progress of pressure-area relationship is conducted since it is one focus of this thesis. At last, the perspective of this thesis is introduced to stress on the difference from previous research.

2.1 Development of the simulation model in this thesis

Before numerical methods come into practice, semi-empirical methods regarding level ice resistance prediction have been proposed since several decades ago. Enkvist (1972) made early studies on full scale and model tests and came up with an analytical breakdown of ice resistance. Lindqvist (1989) presented an easy method of calculating ice resistance and then Riska et al. (1997) gave a simplified version.

Numerical methods have been developed a lot during recent years. Wang (2001) developed a semi-empirical numerical simulation method for conical structures. This model is applied and developed by Su (2011) to simulate ships transiting through level ice with planar motions. The randomness of ice parameters was also considered in his work, being simulated according to the distribution of ice data. The feasibility of this model was discussed in detail by Kuuliala (2015) to see the possibility for actual use. Tan et al. (2013) then expanded the model to 4 and 6 DOFs and discussed the influence of vertical and transverse motions. A pressure-area relationship is also introduced into the model. A modification involving bearing capacity of ice was further conducted by Tan et al. (2014). The bearing capacity is regarded as a function of speed, bending strength, ice thickness and geometry factor. Su et al. (2014) then further developed this model by randomly determining the breaking radius. Zhou (2012) included the force due to rubble accumulation in the total force and proposed another submersion model for comparison. In Zhou et al. (2016), a contact area modification is incorporated into the model based on the theory of an elastic beam resting on an elastic foundation.

2.2 Other methods for ship-ice interaction

Analytical methods are widely used in numerical models. Valanto (2001) developed a theoretical model for the simulation of ice resistance around waterline by modelling the flow around the ship using potential flow theory. Crack propagation is detected by tracking points where the principal stress exceeds the bending strength of ice. Resistance due to underwater part was estimated by Lindqvist's semi-empirical method. Two force peaks within each cycle were identified during the breaking

and rotating processes due to the interaction between ice and hull. Aksnes (2010) introduced a simplified model for moored ships in level ice. The ice-sheet is seen as a semi-infinite elastic beam on an elastic foundation to calculate the breaking force and an energy method is used to calculate the rotating force. Sawamura & Tachibana (2011) derived a new method to calculate the rotating and sliding force based on the theory of an instantaneous impulse. The model can be in 2D or 3D.

Aksnes (2011a and b) presented a panel method to derive ice resistance formula. Ice force signals from measured data are idealised and the force distributions are fitted by statistical methods to construct local ice forces. In Sawamura (2009), finite element method is used to model fluid-ice interaction. Bending failure is the main focus while the forces due to underwater part is neglected in the work.

Real-time simulators can be used in navigation system and for crew training. Motions of ship, water as well as broken ice floes are tracked to reflect real-time environment. This could be computational expensive. Lubbad and Løset (2011) use commercial software physX to solve the equations of rigid body motions in 6 DOFs for all ice floes. The breaking process was detected by tracking the cracks in ice sheet. The broken ice floe can be rebroken during the contact with the ship. Berglund (2012) built an ice fracture model for real-time simulator. The fracture propagation is decided by detecting the weakest direction in the tension field so the shape and size of the broken ice floe is not predetermined.

Ship maneuvering in level ice has also been a focus of researchers. It is also an aim by the model of Su (2011). Lau (2006) used a commercial discrete element code, DECICE, to simulate ships turning in level ice. The physical experiments were carried out using a planar motion mechanism (PMM). Liu et al (2006) derived an analytical method to calculate breaking force, buoyancy force and clearing force during ship maneuvering. A new breaking pattern was also introduced where the broken ice floe was characterized by cusp width and depth.

2.3 Pressure-area relationship

Experimental tests have shown a dependence of ice pressure on contact area. Studies regarding pressure-area relationship have been conducted to provide a better estimation of the impacting force for simulation. Sanderson (1988) presented a plot of data from laboratory strength and indentation tests, impact hammers, offshore platforms, and meso-scale models. It shows a trend of decreasing pressure with increasing area. Masterson et al. (2007) gave a revised pressure-area relationship for isolated small areas according to the results from field measurements. Palmer at al. (2009) then reanalysed this relationship and provided a fracture mechanics explanation. Daley (2007) distinguished the relationship by process and spatial pressre-area relationship, which was confirmed by his data analysis. The results showed that the process relationship follows a rising trend in certain cases, which is in some ways opposite of the usual understanding. Timco (2013) pointed out the mistake in the pressure-area relationship from Sanderson. From his analysis, the measured pressure depends on many ice characters, which includes at least ice strength, aspect ratio, failure mode and interaction rate on ice pressure. The empirical formula is not accurate as it only

takes area factor into consideration. In table 1, a summary of some p-a relationships proposed by researchers are listed. A common feature in these p-a relationships is that they are all in the form of $p = CA^{\alpha}$.

Table 1: Summary of p-a relationships

Sources	Expression	Comment
Masterson & Frederking (1993)	$p = 8.1A^{-0.572}$	up to $19m^2$
Masterson et al. (2007)	$p = 7.4A^{-0.7}$	not contain data on ships in ice
Molikpaq design	$p = 5.119A^{-0.4}$	
Tan et al. (2013)	$p = kA^{n}$	with a reference point (0.1225, 2.3)

2.4 What is new in this thesis

As stated above, numerical simulation of ship transiting and maneuvering in ice has been developed by researchers with several approaches. Validation of the proposed methods are conducted in their papers and it seems that every method gives a nice prediction with great similarities to full scale data. However, it is noticed that these validation are usually conducted by comparing the predicted velocity under certain power output and ice condition with real velocity. Empirical coefficients could be manually altered to fit the reality better. It is found that there exists a large scattering range for the empirical coefficients implemented in different papers. For example, a literature study regarding a coefficient C_f is done by Tan et al. (2014), where it is concluded that C_f has a scattering range from 1.01 to 4.5 by different researchers. This thesis works to evaluate the capacity of predicting resistance and velocity in a time period when power and ice conditions change with time, which fixed empirical coefficients as constant. Thereby we can focus on the assumptions and basis of the model and find solutions to improve its usability. In addition, a resistance component due to ice rubble is calculated and discussed in this thesis, which proves to be an important supplement to the simulation.

3 Resistance prediction methods

In this section, the resistance prediction methods used in this thesis are described in detail. Lindqvist's formula and Riska's formula are semi-empirical methods which give the resistance as a function of ship angles, dimensions, speed and ice properties. Resistance is divided into components due to different phases of ice breaking and then summed up together. The numerical simulation model simulates the resistance component due to crushing and breaking. Then the total resistance is calculated by adding up the resistance due to underwater part, using the formula by Lindqvist (1989).

3.1 Lindqvist formula

Lindqvist (1989) introduced a straightforward ice resistance formula for icegoing ships. The main resistance is categorized as crushing, breaking and submersion resistance with speed dependence. The breaking process is simplified that all forces in the breaking process are generated by crushing the edges of the floes. Both deflection of the ice and trimming of the vessel are ignored.

The average vertical force acting on the ice is estimated as

$$F_v = 0.5 * \sigma_b * h_i^2 \tag{1}$$

where σ_b is the bending strength of the ice, and h_i is the ice thickness. The resistance force due to crushing is then written as:

$$R_c = F_v * \frac{\tan\phi + \mu * \cos\phi / \cos\psi}{1 - \mu * \sin\phi / \cos\psi} \tag{2}$$

where μ is the friction coefficient, ϕ is the stem angle, and ψ is the angle between the normal of the surface and a vertical vector.

As the ship comes into contact with an edge of the ice, the edge is crushed until the contact force is big enough to shear away a small piece of ice. Derived by a mathematical calculation of this process, the breaking resistance is expressed as:

$$R_b = k * B * (h_i^3 / l_c^2) * (\tan\psi + \sin\phi / (\sin\alpha * \cos\phi)) * (1 + 1/\cos\psi) \tag{3}$$

where k is a constant, α is the waterline entrance angle, B is the breadth of the vessel and l_c is the characteristic length of the ice, expressed in equation 4. The formula can be rewritten as equation 5 by replacing the constants:

$$l_c = \left(\frac{E h_i^3}{12(1-\nu^2)\rho_w g} \right)^{\frac{1}{4}} \tag{4}$$

where E is the elastic modulus of ice; ν is the Poisson's ratio; ρ_w is the density of water; g is the acceleration of gravity.

$$R_b = 0.003 * \sigma_b * b * h_i^{1.5} * \left(\tan\psi + \frac{\mu * \cos\phi}{\sin\alpha * \cos\phi} \right) * \left(1 + \frac{1}{\cos\psi} \right) \tag{5}$$

from which the resistance is proportional to the ice thickness to the power of 1.5.

The broken ice floe will be further turned and submerged under ship hull. Based on mathematical calculations, the resistance due to submersion and friction is written as

$$R_s = \delta\rho * g * h_i * \left(T * \frac{B+T}{B+2*T} + \mu * (A_u + \cos\phi * \cos\psi * A_f)\right) \tag{6}$$

where $\delta\rho$ is the density difference between the water and the ice; g is the gravitational constant; h_i is the ice thickness; L, B and T are the length, breadth and draught of the ship; μ is the friction coefficient; A_u is the area of the flat bottom and A_f is the area of the bow. Using approximations for the area of the surfaces, it is obtained that

$$R_s = \delta p * g * h_i * \left(T * \frac{B+T}{B+2*T} + \mu * \left(0.7 * L - \frac{T}{\tan\phi} - \frac{B}{4*\tan\alpha} + T * \cos\phi * \cos\psi * \sqrt{\frac{1}{\sin\phi^2} + \frac{1}{\tan\alpha^2}}\right)\right) \tag{7}$$

Speed is another factor influencing the resistance. The breaking resistance can increase if floe size decreased with increasing speed. The speed will clearly influence the flow lines of the broken ice and the submersion component will therefore change with the speed. The friction can also increase because of the dynamic water pressure.

The resistance is found to increase fairly linearly with the speed. Using two empirical constants the total ice resistance is obtained

$$R_i = (R_c + R_b) * \left(1 + 1.4 * \frac{v}{\sqrt{g * h_i}}\right) + R_s * \left(1 + 9.4 * \frac{v}{\sqrt{g * L}}\right) \tag{8}$$

3.2 Riska's formula

Riska et al. (1997) pointed out the the level ice resistance arises when a ship breaks ice floes from the intact ice field, turns them parallel to the ship and forces them to slide down and eventually up along the hull. The parameters which ice resistance depends on are divided into three groups. The first group consists of the external variables: ice thickness h_i and ship speed v. The two other groups contain the shape of the ship (ϕ, B/T, L/B, L_{bow}/L, L_{par}/L) and the size of the ship (L, B, T). The ice resistance is:

$$R_i = f(h_i, v; \phi, \frac{B}{T}, \frac{L}{B}, \frac{L_{bow}}{L}, \frac{L_{par}}{L}, B, T, L) = C_1 + C_2 v \tag{9}$$

The constants C_1 and C_2 are expressed as

$$C_1 = f_1 \frac{1}{2\frac{T}{B}+1} B L_{par} h_i + (1 + 0.021\phi)(f_2 B h_i^2 + f_3 L_{bow} h_i^2 + f_4 B L_{bow} h_i) \tag{10}$$

$$C_2 = (1 + 0.063\phi)(g_1 h_i^{1.5} + g_2 B h_i) + g_3 h_i (1 + 1.2\frac{T}{B})\frac{B^2}{\sqrt{L}} \tag{11}$$

where f_i and g_i are constants. Their values are listed in table 2.

Table 2: The constants used in Riska's formula (Riska et al. 1997)

f_i	g_i
$f_1 = 0.23kN/m^3$	$g_1 = 18.9kN/(m/s \cdot m^{1.5})$
$f_2 = 4.58kN/m^3$	$g_2 = 0.67kN/(m/s \cdot m^{1.5})$
$f_3 = 1.47kN/m^3$	$g_3 = 1.55kN/(m/s \cdot m^{1.5})$
$f_4 = 0.29kN/m^3$	

3.3 Numerical simulation model

Ice breaking process is modelled and simulated by Su (2011) using a semi-empirical method in planar motions. The process can be divided into several stages. First, the ship encounters the ice sheet and crushing happens. (Su 2011) The crushing force will keep increasing with growing contact area until the vertical component is large enough to cause a bending failure, after which the broken ice floe will be turned by the ship until parallel to the hull. (Su 2011) Then it is submerged with the advancing of the ship and slides along the ship hull and finally it is cleared at the aft of the ship. (Su 2011)

Crushing and breaking stages are modelled and simulated by this method, while the resistance due to underwater part is estimated according to Lindqvist's method. The contact is assumed to be at the waterline, which is discretized into a closed polygon and the edge of the ice is discretized into a polyline in the simulation program, shown in Figure 2.

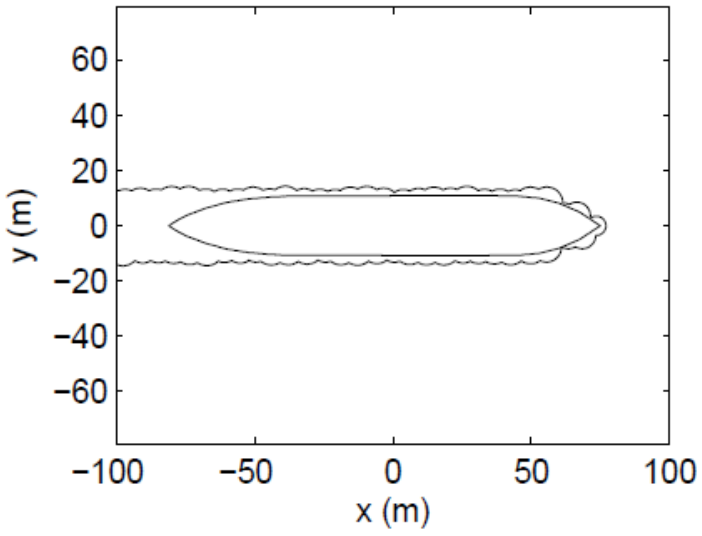

Figure 2: Discretization of ship and ice edges into polygons and polylines (Kuuliala 2015)

3.3.1 Crushing force

As shown in Figure 2, the ship waterline and ice sheet edge are discretized. At each time step, an algorithm can detect the ice nodes inside the ship polygon, which determines the contact area between ship and ice. The contact surface is assumed to be flat. The area, A_c, is simply determined by the contact length L_h, and the indentation depth, L_d. As shown in Figure 3, two cases must be considered in the calculation of contact area

$$\begin{aligned} A_c &= \frac{1}{2} L_h \frac{L_d}{\cos\phi} && Case1 : L_d tan\phi \leq h_i \\ A_c &= \frac{1}{2}(L_h + L_h \frac{L_d - h_i/\tan\phi}{L_d} \frac{h_i}{\sin\phi}) && Case2 : L_d tan\phi > h_i \end{aligned} \tag{12}$$

where h_i is the ice thickness, ϕ is a slope angle of varying values at different hull zones.

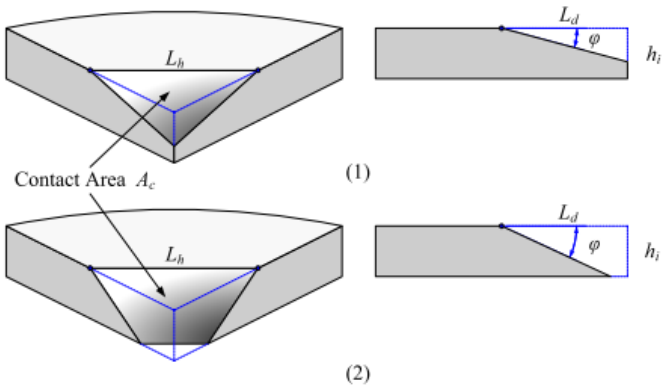

Figure 3: Two cases of contact area (Su 2011)

The ice crushing force in Su's model is by multiplying the contact surface area A_c and the effective ice crushing strength, σ_c:

$$F_{cr} = \sigma_c \cdot A_c \tag{13}$$

where the effective ice crushing strength is a constant during crushing process.

However, many researches show that the pressure on the contact area varies with changing area. Generally, there is a pressure-area relationship which can be stated in this form:

$$p_c = C A_c^a \tag{14}$$

where C and a are constants. Kuuliala (2015) used crushing strength for C and set a to be -0.4. Then crushing force is

$$F_{cr} = \sigma_c A_c^{0.6} \tag{15}$$

In this thesis, both methods are discussed and compared to the full scale data.

Friction force can be divided into horizontal and vertical parts. According to the relative motion between ice and hull, the components can be expressed as:

$$f_H = \mu_i \cdot F_{cr} \cdot \frac{v_t^{rel}}{\sqrt{(v_t^{rel})^2 + (v_{n,l}^{rel})^2}} \tag{16}$$

$$f_H = \mu_i \cdot F_{cr} \cdot \frac{v_{n,l}^{rel}}{\sqrt{(v_t^{rel})^2 + (v_{n,l}^{rel})^2}} \tag{17}$$

where μ_i is the frictional coefficient, v^{rel} is the relative velocity between ice and hull, as shown in Figure 4.

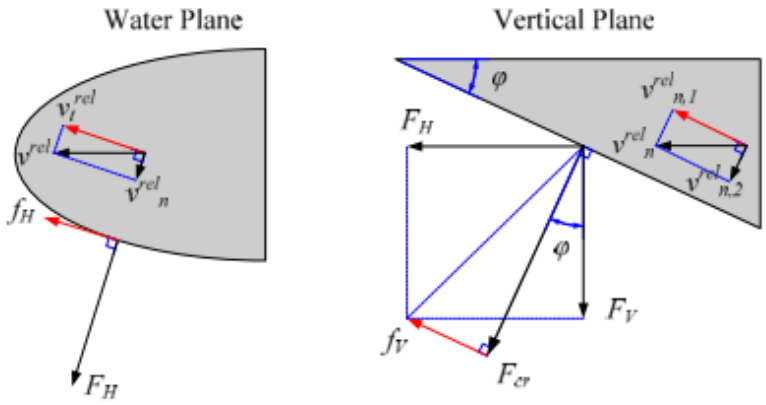

Figure 4: Forces and velocities decomposion (Su 2011)

Then the horizontal and vertical components of the total contact force can be written as:

$$F_H = F_{cr} \cdot \sin\phi + f_v \cdot \cos\phi \tag{18}$$

$$F_V = F_{cr} \cdot \cos\phi + f_v \cdot \sin\phi \tag{19}$$

Zhou et al. (2016) proposed a crushing force adjustment based on ice plate flexural deflection. The actual ship-ice contact is seen as a dynamic process where the crushing force and ice plate flexural deflection influence each other. After the contact with ship, ice will be suppressed due to the vertical force. The real contact area will be less than that detected by the algorithm, which gives less contact force. Water underneath the ice sheet can be seen as elastic foundation which gives support to ice plate deflection.

As shown in 5, the ship has advanced a distance of δ_s since the contact with ice. The ice sheet is suppressed by δ_e and the real crushing heigh is δ_c. The following relationship exists:

$$\delta_e + \delta_c = \delta_s / \tan\phi \tag{20}$$

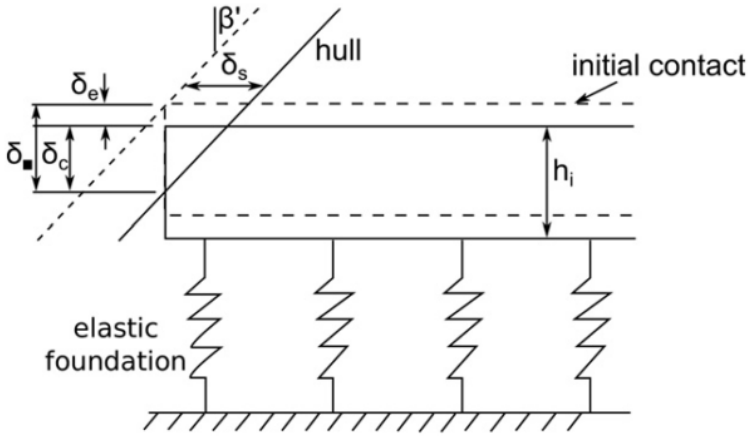

Figure 5: Flexual deflection of ice plate (Zhou et al. 2016)

Considering a vertical force acting on the apex of a homogeneous and isotropic elastic ice plate resting on a liquid support with an open angle of θ, the deflection is expressed as equation 21.

$$w_0 = \frac{1}{2}\left(\frac{\pi}{\theta}\right)^2 \frac{P}{\sqrt{\gamma D}} \tag{21}$$

where P is the concentrated load; $\gamma = \rho_w g$ is the weight per unit volume; $D = Eh_i^3/(12(1-\nu^2))$ is the flexural rigidity of ice plate; E is the ice Young's modulus; ν is Poisson's ratio. Replacing P and w_0 by F_V and δ_e, the following relationship is given

$$F_V = \frac{2\theta^2}{\pi^2}\sqrt{\rho g D}\delta_e \tag{22}$$

From this δ_e, the contact area can be modified by multiplying an adjustment coefficient $(\delta_c/\delta_v)^2$. This will give a new crushing force and then a new δ_e. By iteration, it is able to find the real contact area and crushing force.

3.3.2 Ice bending failure

The ice sheet will be broken when the vertical force grows to exceed the bending capacity of the ice sheet, P_f. Su gives the expression of P_f as:

$$P_f = C_f\left(\frac{\theta}{\pi}\right)^2 \sigma_f h_i^2 \tag{23}$$

where θ is the opening angle of the idealized ice wedge shown in Figure 6, σ_f is the flexural strength of the ice, h_i is the thickness of the ice, and C_f is an empirical parameter, which must be obtained from measurements.

Tan et al. (2014) pointed out that the bending failure load of an ice wedge subjected to a rapid loading increases with increasing loading rates. So C_f should be dependent on the advancing velocity. A non-dimensional analysis is carried out

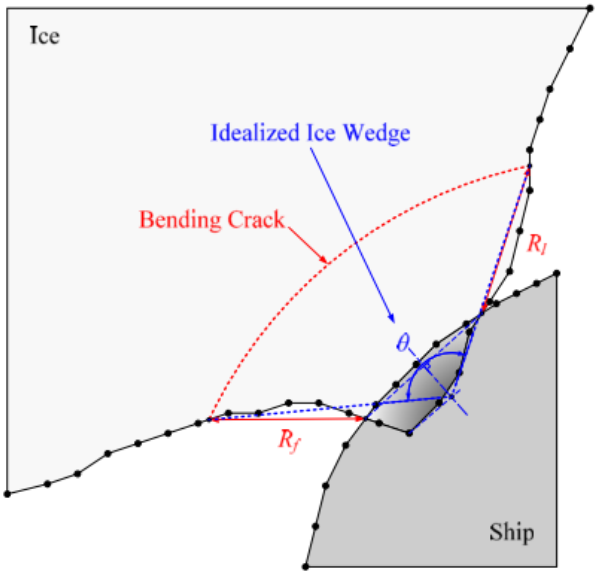

Figure 6: Idealized ice-hull contact (Su 2011)

assuming that the dynamic bearing capacity, P_f, is proportional to the bending strength (σ_f), the square of thickness (h_i^2) of the ice, and the geometry factor, $((\frac{\theta}{\pi})^2)$, specifying the wedge size in the circumferential dimension. The result is expressed numerically as:

$$P_f(v_2) = (1.65 + 2.47v_2^{0.40})\sigma_f h_i^2(\frac{\theta}{\pi})^2 \tag{24}$$

Here v_2 is the relative normal velocity of the contact plane. Both bending failure criteria are discussed and compared to full scale data in this thesis.

3.3.3 Ice breaking pattern

When the vertical force exceeds the bearing capacity of the ice wedge, ice will be broken. The shape of broken ice floes is quite random and irregular. For simplicity use in the model, ice floes are idealized as a sector area which has a certain radius with the centre at the centroid of the contact area. Two different ways to decide the floe radius are presented here.

Deterministic crack size The broken ice floe is idealized for the convenience of simulation. According to Wang (2001), the bending crack is determined by the interpolation of the icebreaking radius at the first and last contact node, shown in Figure 6. The radius R is given as

$$R = C_l \cdot l_c \cdot (1.0 + C_v \cdot v_{n,2}^{rel}) \tag{25}$$

where $v_{n,2}^{rel}$ is the relative normal velocity between the contact surface and the hull node; l_c is the characteristic length of the ice given by equation 4; C_l and C_v are two empirical parameters obtained from field measurements. C_l determines the floe

radius in zero speed and C_v gives its dependence of advancing speed. Wang used $C_l = 0.32$ and $C_v = -0.14$ in her simulation for a conical structure.

Random crack size Su et al. (2014) introduced a random crack size model into the method based on the work of Izumiyama et al. (1992). Crack size is regarded as a random value which is normally distributed around a mean value. According to Izumiyama et al. (1992), the distribution has a mean value of 0.94 and a standard deviation of 0.27, determined based on the observed crack pattern in the model test. Su then adopted the R value according to Wang (2011) as the mean value R_m and used the same ratio between mean value and standard deviation from Izumiyama et al. (1992), which gives standard deviation $R_{sd} = 0.287R$. Then a random crack radius is generated by using:

$$\begin{aligned} F(R) &= \frac{1}{\sqrt{2\pi R_{sd}}} \cdot \int_0^R \exp\left(\frac{-(s-R_m)^2}{2R_{sd}^2}\right) \dot{ds} \\ U &\sim U(0,1) \\ R &= F^{-1}(U) \end{aligned} \tag{26}$$

where $F(R)$ is the cumulative distribution function (CDF) of the crack radius, $F^{-1}(U)$ is the inverse CDF, and U is a randomly generated number between 0 and 1. (Su et al. 2014)

3.3.4 Ship's motion (Su 2011)

Considering only planar motion, in global coordinate system, planar motion of a ship can be described as:

$$\begin{aligned} m\dot{u}_g &= FX_g \\ m\dot{v}_g &= FY_g \\ I_z\dot{r} &= N \end{aligned} \tag{27}$$

where FX_g, FY_g are the forces in surge and sway directions; N is the yaw moment; m is the mass of the ship; I_z is the moment of inertia in yaw direction; u_g, v_g and r are the velocities in surge, sway and yaw respectively. The dot notation denotes the derivative with respect to time. In ship coordinate system, these can be rewritten as:

$$\begin{aligned} FX_g &= FX\cos\Psi - FY\sin\Psi \\ FY_g &= FX\sin\Psi + FY\cos\Psi \end{aligned} \tag{28}$$

$$\begin{aligned} u_g &= u\cos\Psi - v\sin\Psi \\ u_g &= u\sin\Psi + v\cos\Psi \end{aligned} \tag{29}$$

where Ψ is the heading angle of the ship, shown in Figure 7.

The accelerations in the ship coordinate system are obtained by differentiating equation 29

$$\begin{aligned} \dot{u}_g &= \dot{u}\cos\Psi - \dot{v}\sin\Psi - (u\sin\Psi + v\cos\Psi)r \\ \dot{u}_g &= \dot{u}\sin\Psi - \dot{v}\cos\Psi - (u\cos\Psi + v\sin\Psi)r \end{aligned} \tag{30}$$

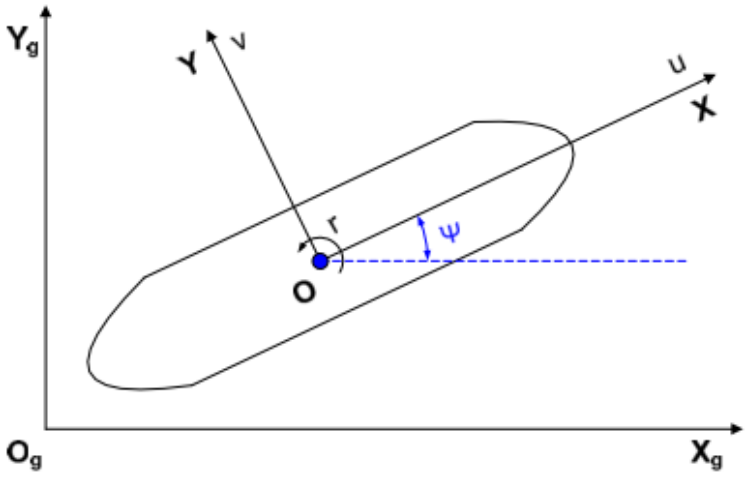

Figure 7: Ship coordinate system (Su 2011)

The ship's motion in ship coordinate system can then be described by

$$\begin{aligned} m \cdot \dot{u}_g &= FX + m \cdot v \cdot r \\ m \cdot \dot{v}_g &= FY - m \cdot u \cdot r \\ I_z \cdot \dot{r} &= N \end{aligned} \tag{31}$$

Using a general matrix form, the equations can be written in this form

$$(\mathbf{M} + \mathbf{A}\cdot)\ddot{\mathbf{x}}(t) + \mathbf{B} \cdot \ddot{\mathbf{x}}(t) = \mathbf{F}(t) \tag{32}$$

where the hydrodynamic coefficients are calculated according to regression formulas.

3.3.5 Excitation forces

The forces acting on the ship include those from ice, propeller, rudder and open water, expressed as follows:

$$F_1 = F_1^i + F_1^p + F_1^r + F_1^{ow} + m \cdot v \cdot r \tag{33}$$
$$F_2 = F_2^i + F_2^p + F_2^r + F_2^{ow} - m \cdot u \cdot r \tag{34}$$
$$F_6 = F_6^i + F_6^p + F_6^r + F_6^{ow} \tag{35}$$

where the subscripts 1, 2 and 6 refer to the directions of surge, sway and yaw, the superscripts i, p, r and ow refer to the ice, propeller, rudder and open water respectively. Since the ship simulated in this thesis goes in a straight line, rudder force can be taken as zero.

Ice forces Ice forces due to breaking ice are simulated according to the method described in sub-section 3.3.1. Turning, submerging and sliding forces are calculated from the ice resistance formula derived by Lindqvist (1989). In addition to these

forces implemented in Su's model, in this thesis, a ridge resistance formula is applied for the forces due to possible ice rubble. Rubble thickness are derived from the difference between EM and stereo camera measured ice thickness. Resistance due to these ice rubble is calculated by a ridge resistance formula from Riska et al. (1997) based on Malmberg (1983)

$$R_r = C_1 T h_r (\frac{B}{2} + h_r \tan\Psi \cos\alpha)(0.15\cos\alpha + \sin\Psi\sin\alpha) + C_2 T L_{par}[0.27 h_r + (\frac{h_r}{T} - \frac{1}{2})B] \tag{36}$$

where the constants are $C_1 = 7500N/m^3$ and $C_2 = 172N/m$; h_r is the ridge thickness; the factor $\frac{H_r}{T} - \frac{1}{2}$ is non-negative. The other symbols are defined same as before.

Thus the 3DOF ice force components can be expressed by

$$F_1^{ice}(t) = F_1^{brk}(t) + (R_s(1 + 9.4\frac{v^{rel}}{\sqrt{gL_{WL}}}) + R_r) * \frac{v_1^{rel}}{v^{rel}} \tag{37}$$

$$F_2^{ice}(t) = F_2^{brk}(t) + (R_s(1 + 9.4\frac{v^{rel}}{\sqrt{gL_{WL}}}) + R_r) * \frac{v_2^{rel}}{v^{rel}} \tag{38}$$

$$F_6^{ice}(t) = F_6^{brk}(t) \tag{39}$$

where R_s is the submersion component of ice resistance given by Eq. 7; v_1^{rel} and v_2^{rel} are respectively the forward and transverse components of the relative velocity between ship and ice; L_{WL} is the ship water line length.

Propeller thrust Net thrust is a concept used in ship-ice interaction, denoting the thrust available to overcome ice resistance. It is defined as the difference between ship thrust and open water resistance at given speed. In the ice rules, the net thrust available to overcome ice resistance can be estimated as

$$T_{net} = T_B \left(1 - \frac{1}{3}\frac{v_1^{rel}}{v_{ow}} - \frac{2}{3}(\frac{v_1^{rel}}{v_{ow}})^2\right) \tag{40}$$

where T_B is the bollard pull; v_{ow} is open water speed; v_1^{rel} is the forward component of the relative velocity between ship and ice.

Since there is no data regarding the bollard pull of the modelled ship available, an estimation is conducted based on propulsive power and propeller dimension by

$$T_B = K_E(PD)^{2/3} \tag{41}$$

where K_E is an empirical factor; P is the power in kilowatts; D is the propeller diameter in meters. T_B is in kilonewtons. Values of K_E is given in table 3. (Kujala and Riska 2010)

During the full scale measurements of the modelled ship, it made three ahead tests under full, medium and low power respectively. Since there is no data available regarding power-open water speed relationship, an estimation is done to find the open water speed under different power. The estimation is done according to Admiralty

Table 3: Values of K_E.(Kujala and Riska 2010)

	Controllable pitch	**Fixed pitch**
Single propeller	0.78	0.87
Twin propeller	0.98	1.09
Triple propeller	1.12	1.24

Coefficient, which is an old method used in early stage ship design to estimate ship power. For the same ship, its admiralty coefficient C is constant

$$C = \frac{\sqrt[3]{\Delta^2} \cdot v^3}{P} \tag{42}$$

where Δ is the displacement of the ship in tonnes; v is ship speed under a certain power P (in horsepower). From this relationship, the open water speed v_P under a power of P could be expressed as

$$v_P = \left(\frac{P}{P_{full}}\right)^{1/3} \cdot v_{full} \tag{43}$$

where P_{full} is the full power of the ship and v_{full} is the speed under this power.

With equation 41, 43 and table 3, the net thrust under any speed is achieved.

Hydrodynamic forces Hydrodynamic forces can be measured by model experiment or calculated by strip method or computational hydrodynamics method once given detailed ship line drawings. Due to the limitation of available data, an empirical method is used to estimate the hydrodynamic derivatives.

Assuming a linear dependence of hydrodynamic forces on velocity, forces in the second and sixth degrees of freedom (sway and yaw) can be expressed as

$$\begin{aligned} Y &= Y_{\dot{v}}\dot{v} + Y_v v + Y_{\dot{r}}\dot{r} + Y_r r \\ N &= N_{\dot{v}}\dot{v} + N_v v + N_{\dot{r}}\dot{r} + N_r r \end{aligned} \tag{44}$$

where for example $Y_v v$ is the force in y-direction due to sway velocity. $Y_{\dot{v}}\dot{v}$ and $N_{\dot{v}}\dot{v}$ correspond to the added mass of sway and yaw motion while $Y_v v$ and $N_v v$ correspond to damping coefficients. x-direction terms are negligible in magnitude for Y and N. X_u is not needed because it is already included in net thrust model. Therefore, the hydrodynamic coefficients in equation 32 are

$$A = \begin{bmatrix} 0 & 0 & 0 \\ 0 & Y_{\dot{v}} & Y_{\dot{r}} \\ 0 & N_{\dot{v}} & N_{\dot{r}} \end{bmatrix} \tag{45}$$

$$B = \begin{bmatrix} 0 & 0 & 0 \\ 0 & Y_v & Y_r \\ 0 & N_v & N_r \end{bmatrix} \tag{46}$$

Linear seakeeping theory in this thesis is only applicable for small drift angles. Due to the shortage of available data, more accurate methods can not be applied here. Matusiak (2013) made a regression of the results from model test to estimate the non-dimensional hydrodynamic derivatives, which are given in the following equations

$$\begin{aligned}
Y'_{\dot{v}'} &= -\pi(T/L)^2(1 + 0.16C_B B/T - 5.1(B/L)^2) \\
Y'_{\dot{r}'} &= -\pi(T/L)^2(0.67B/L - 0.00033(B/T)^2) \\
N'_{\dot{v}'} &= -\pi(T/L)^2(1.1B/L + 0.0003341B/T) \\
N'_{\dot{r}'} &= -\pi(T/L)^2(1/12 + 0.0176C_B B/T - 0.33B/L) \\
Y'_{v'} &= -\pi(T/L)^2(1 + 0.4C_B B/T) \\
Y'_{r'} &= -\pi(T/L)^2(-0.5 + 2.2B/L - 0.08B/T) \\
N'_{v'} &= -\pi(T/L)^2(0.5 + 2.4T/L) \\
N'_{r'} &= -\pi(T/L)^2(0.25 + 0.039B/T - 0.56B/L)
\end{aligned} \tag{47}$$

Once non-dimensional derivatives are calculated, dimensional derivatives are achieved for each time step based on ship velocity, density of water and length of the ship.

3.4 Solver for equations of motion

The equations are solved by a step-by-step numerical integration method according to Newmark's method (Newmark 1959). The goal is to solve equation 32 for every time step. The excitation force $F(t)$ is dependent on the position and velocity of the ship. Thus it can be rewritten as

$$(\mathbf{M} + \mathbf{A}\cdot)\ddot{\mathbf{x}}(t) + \mathbf{B} \cdot \ddot{\mathbf{x}}(t) = \mathbf{F}(x(t), x(\dot{t})) \tag{48}$$

where the mass matrix and position vector are

$$\mathbf{M} = \begin{bmatrix} m & 0 & 0 \\ 0 & m & 0 \\ 0 & 0 & I_{zz} \end{bmatrix} \quad \text{and} \quad \mathbf{x} = \begin{bmatrix} X_G \\ Y_G \\ \Psi \end{bmatrix} \tag{49}$$

According to Newmark's method, at time step $k+1$, there is the relationship

$$\dot{\mathbf{x}}(t_{k+1}) = \mathbf{x}(t_k) + (1-\lambda)\ddot{\mathbf{x}}\delta t + \lambda\ddot{\mathbf{x}}(t_{k+1})\delta t \tag{50}$$

$$\mathbf{x}(t_{k+1}) = \mathbf{x}(t_k) + \dot{\mathbf{x}}(t_k)\delta t + \left(\frac{1}{2} - \beta\right)\ddot{\mathbf{x}}(t_k)\delta t^2 + \beta\ddot{\mathbf{x}}(t_{k+1})\delta t^2 \tag{51}$$

A linear relationship is convenient for computation. To satisfy the linearity, λ and β should be $1/2$ and $1/6$ respectively in order to give a linear acceleration. (Newmark 1959) The equations then become

$$\dot{\mathbf{x}}(t_{k+1}) = \dot{\mathbf{x}}(t_k) + \frac{1}{2}\ddot{\mathbf{x}}\delta t + \frac{1}{6}\ddot{\mathbf{x}}t_(k+1)\delta t \tag{52}$$

$$\mathbf{x}(t_{k+1}) = \mathbf{x}(t_k) + \dot{\mathbf{x}}(t_k)\delta t + \frac{1}{3}\ddot{\mathbf{x}}(t_k)\delta t^2 + \frac{1}{6}\ddot{\mathbf{x}}(t_{k+1})\delta t^2 \tag{53}$$

At time step k+1, the acceleration is

$$\ddot{\mathbf{x}}(t_{k+1}) = (\mathbf{M} + \mathbf{A})^{-1}\mathbf{F}(t_{k+1}) \tag{54}$$

Inserting equation 54 into equation 52 and 53, the position vector at k+1 step can be expressed as

$$\mathbf{x}(t_{k+1}) = \left(\frac{6}{\delta t^2}(\mathbf{M} + \mathbf{A}) + \frac{3}{\delta t}\mathbf{B}\right)^{-1} (\mathbf{F}(t_{k+1}) + (\mathbf{M} + \mathbf{A})\mathbf{a}_k + \mathbf{B}\mathbf{b}_k) \tag{55}$$

where $\mathbf{a_k}$ and $\mathbf{b_k}$ are given by

$$\mathbf{a}_k = \frac{6}{\delta t^2}\mathbf{x}(t_k) + \frac{6}{\delta t}\dot{\mathbf{x}}(t_k) + 2\ddot{\mathbf{x}}(t_k) \tag{56}$$

$$\mathbf{b}_k = \frac{3}{\delta t}\mathbf{x}(t_k) + 2\dot{\mathbf{x}}(t_k) + \frac{1}{2}\ddot{\mathbf{x}}(t_k)\delta t \tag{57}$$

Equation 55 can not be solved directly because the excitation force at k+1 step depends on the position and velocity at the same step. Iteration is called to solve this. Assuming a constant acceleration, the position and velocity can be calculated as

$$\mathbf{x}^0(t_{k+1}) = \mathbf{x}(t_k) + \dot{\mathbf{x}}(t_k)\delta t + \frac{1}{2}\ddot{\mathbf{x}}(t_k)\delta t \tag{58}$$

$$\dot{\mathbf{x}}^0(t_{k+1}) = \dot{\mathbf{x}}(t_k) + \ddot{\mathbf{x}}(t_k)\delta t \tag{59}$$

The iteration is started by calculating excitation with position and velocity given by equation 58 and 59. New value for the position is calculated using equation 55 and velocity is updated using equation 52. These new values are then used to determine excitation for the next iteration round. The iteration is continued until the change in the excitation from one iteration to the next is small enough. The stopping criterion is

$$\frac{||\mathbf{F}(t_{k+1}) - \mathbf{F}(t_k)||}{||\mathbf{F}(t_k)||} < \epsilon \tag{60}$$

where ϵ is of the order 10^{-3}. (Kuuliala 2015)

4 Ice thickness measurement methods and preliminary data analysis

The data used for evaluation in this thesis is from full scale test of icebreaker S.A. Agulhas II. During her ice trial on Baltic sea in March 2012, several tests were conducted for the aim of research use. Test results includes ice thickness data, speed and power output during the sailing. The test is divided into several scenarios, with full, medium and low power respectively. In this chapter, measurement methods onboard this ship are firstly introduced. Following that the achieved data are preliminarily analysed and organised in a way that is representative and easy to input.

4.1 Measurement methods

Three ice thickness measurement methods were implemented during the test of S.A. Agulhas II, namely visual observation, electromagnetic system and stereo camera method. These methods use different technologies and give different results. The aim of this part is to look into the mechanism of these methods in order to better understand the data and put it into use.

4.1.1 Visual observation

Visual observation is conducted by observers during this ice trial. A measurement stick is installed at the side of a ship, with 10 cm division. It is located between the ice and the observers. People in the bridge can use it as a reference to estimate the ice thickness when the ice is turned upright by the ship. Onboard S.A. Agulhas II, visual observation have been made by recording approximate histograms of ice observed during 10-minute time periods. (Suominen et al.2014) What is obtained hereby is a coarse estimate of the whole thickness distribution during the 10 minute period. (Lensu et al. 2015) This time resolution is essential for mapping ice properties to navigational parameters., but comes at a cost of poor quality of thickness reading as the histogram bins might be 20 - 40 cm or wider. Moreover this method requires one person to concentrate solely on ice observations. (Kulovesi & Lehtiranta 2014)

4.1.2 EM method

The EM31 is a man-portable instrument designed to measure apparent ground conductivity by means of electromagnetic induction. (Kovacs & Morey 1991) It has a transmitter (Tx) and a receiver (Rx) coil that function as magnetic dipole antennae. (Kovacs & Morey 1991) The EM31 is designed to measure the magnitude of the in-phase and quadrature components of the secondary magnetic field. (Kovacs & Morey 1991)

According to Kovacs & Morey (1991), EMI sounding does not give a point measurement but provides an ”average” ice thickness for an area having a diameter of about three times the height of the instrument above the seawater. Unsatisfactory

ice thickness measurements were generally obtained in areas of deformed ice where the measured electromagnetic response was adversely affected by conductive inhomogeneities associated with the submerged ice block structure. (Kovacs & Morey 1991)

The EM thickness measurement system onboard S.A. Agulhas II is composed of a Geonics EM-31 electromagnetic conductivity sounder and a laser distance meter in a protective cover. (Lensu et al. 2015) The two instruments measure distance to the ice underside and to the ice or snow surface respectively. The difference yields then combined thickness of ice and snow layers. The data from the thickness measurement system includes GPS data, laser distance to ice or snow surface, laser signal amplitude measuring the relative strength of the returning laser signal, apparent conductivity recorded by the EM device. (Lensu et al. 2015)

4.1.3 Stereo camera method

Researchers from Aalto university developed a semi-automatic machine vision based tool named stereo camera method to measure level ice thickness. (Kulovesi & Lehtiranta 2014) This stereo configuration allows reliable 3D measurement of ice dimensions. Human input is needed for choosing feasible cases. (Kulovesi & Lehtiranta 2014) The presented computer program then detects edges and automatically calculates ice thickness. The process is monitored and results verified by the human operator. (Kulovesi & Lehtiranta 2014)

Compared to visual observation, this approach can reduce human effort in post-processing stage and greatly reduce subjectivity due to employing computer vision methods for critical measurement sub-tasks (Kulovesi & Lehtiranta 2014). However, according to Kulovesi & Lehtiranta (2014), there are also limitations with this approach. Only overturned blocks will ever be seen and measured with this principle. Thus, only such level ice can be measured that is sufficiently rigid to turn. Additionally, the ship's ice breaking properties set a limit to how thick blocks of ice it can turn. Consequently, a selection bias is at play - not all ice is measured and the probability of ice getting measured depends on its properties. (Kulovesi & Lehtiranta 2014)

4.1.4 Comparison among measurement methods

A comparison among visual observation, EM device and stereo camera methods have been conducted in Suominen et al. (2014) based on full scale test onboard S.A. Agulhas II. Several conclusions have been drawn. Visual observation tends to overestimate ice thickness compared to stereo camera. The data shows weak correlation between EM and stereo camera data. This is because that the EM system seeks measures the total thickness of the ice mass within its range of penetration, while the stereo camera system quantifies the thickness from upturning ice pieces. (Suominen et al. 2014)

It is also concluded that the probability density distribution of EM measured thickness is a normal-exponential distribution while stereo camera measured thickness shows normality. Suominen et al. (2014) then mentioned that the exponential signal

is due to ice ridges and gradually disappears for averages in longer length scales and the distribution turns normal.

4.2 Preliminary data analysis

Full scale data are used to validate the aforementioned models. The data were collected by a polar supply and research vessel, S.A. Agulhas II, during maneuver tests in an level ice field in Baltic Sea. (Bekker et al. 2014) EM device and stereo camera were installed onboard this ship to measure the ice thickness during the voyage. Descriptions about the test plan are presented in Bekker et al. (2014). The ship sailed along a route according to the plan, which is shown in Figure 8.

The data used in this thesis are those from the moving ahead parts. It contains the ice thickness data from EM and stereo camera measurements, ship speed and power output. Each scenario corresponds to a set of data from a five to six minutes period.

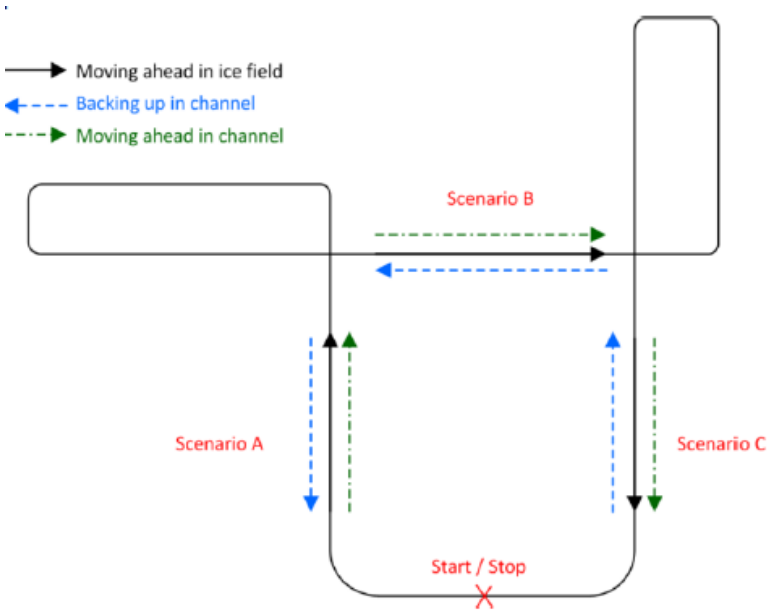

Figure 8: Planned ship sailing route (Bekker et al. 2014)

4.2.1 Ice thickness data

Figure 9 shows the scatter plots of the thickness data from EM measurement and stereo measurement together with 3 seconds averaged thickness line. It can be seen that EM measurement has a much higher sample rate during the same time period. The thickness mostly ranges from 0 to 1.5 metres in EM data, while in stereo camera data it narrows mainly between 0 and 0.4 metres, which is quite different from EM data. As discussed in the former section, difference between EM and stereo camera data usually consists of snow thickness and ice rubble thickness. Although this ice field is classified as level ice according to Bekker et al. (2014), there is still significant

ice rubble accumulation according to the measurements. Specifically, at 0-120th second and 170th-300th second under full power, 50th-90th second, 140th-150th second and 200th-280th second under medium power, 0th-170th second under low power, ice rubble is clearly seen from the figure. These ice rubble will contribute to ice resistance as will be shown by simulation results. Besides, stereo camera measured ice thickness in medium and low power does not vary much, fluctuating around 0.3 metres. In full power case, ice thickness is only 0.1m from 120s to 160s. According to the ship route figure, the measured ices are in an area of no more than 2km×2km. Therefore ice properties can be assumed the same within this area.

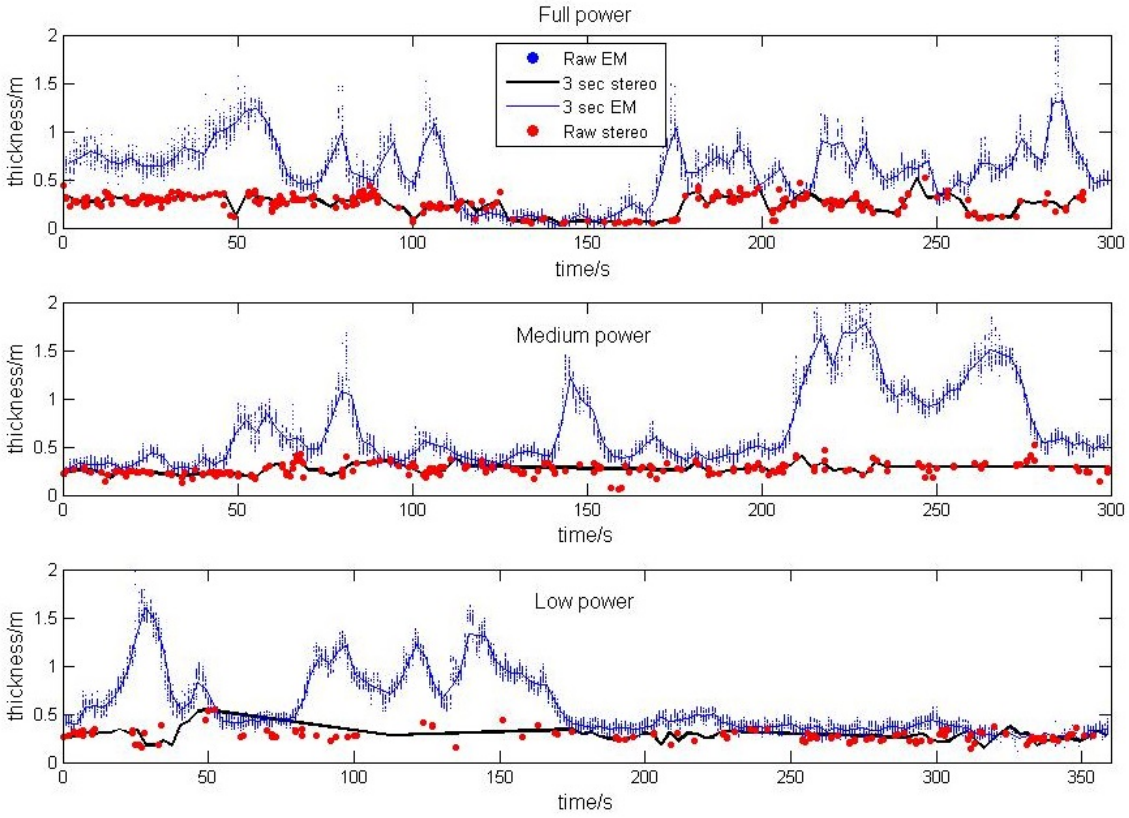

Figure 9: EM and stereo camera measured ice thickness with full, medium and low power, raw data and 3 seconds averaged data presented

Figure 10 and figure 11 give the histograms of thickness data given by the two measurements. According to the visual observation results from Bekker et al. (2014), 60% of the observed ice floes have a thickness between 10 and 30 cm and the other 40% are between 30 and 70 cm. It is obvious that the stereo camera data gives more close percentage while EM data are far beyond these ranges. This indicates that the stereo camera data is more reliable in predicting level ice thickness. Thus it could be used in the simulation as level ice thickness.

The thickness data from stereo camera can be fitted quite well by normal distribution, which is consistent with the results of Suominen et al. (2014). The fitted distribution curves are drawn in Figure 11. The mean values and standard devia-

tions are [0.26,0.094], [0.27,0.063] and [0.28,0.063]. EM thickness data, according to Suominen et al. (2014), fit a normal-exponential distribution since it also includes ice rubble thickness.

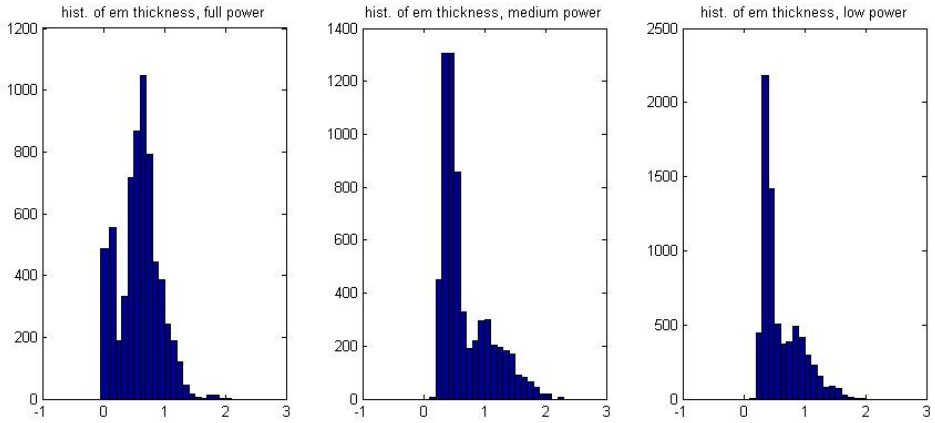

Figure 10: Histogram of EM measured ice thickness

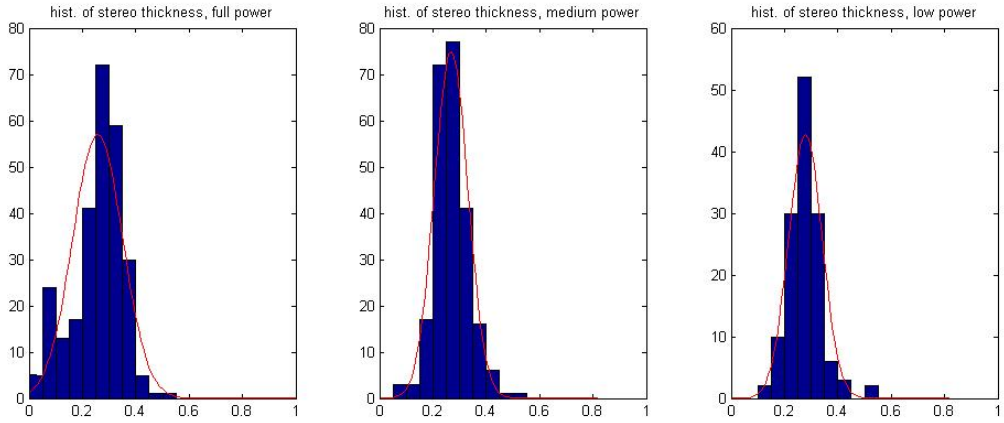

Figure 11: Histogram of Stereo camera measured ice thickness

Since stereo camera measured thickness does not show great changes for the time period during each test, the data is averaged into 30 seconds intervals for simplicity. The averaged results are plotted in figure 12, where ice rubble thickness is derived by subtracting stereo camera thickness from EM thickness. Ice rubble thickness is also average into 30 seconds intervals in this figure for comparison. However, since rubble thickness changes quite fast with time moving on, in the simulation, it is averaged every 5 seconds to retain necessary information.

4.2.2 Speed and power data

Figure 13 shows the power output scaled by set power during the test. According to Bekker et al. (2014), the powers are set to be 5000kW, 2600kW and 1900kW for

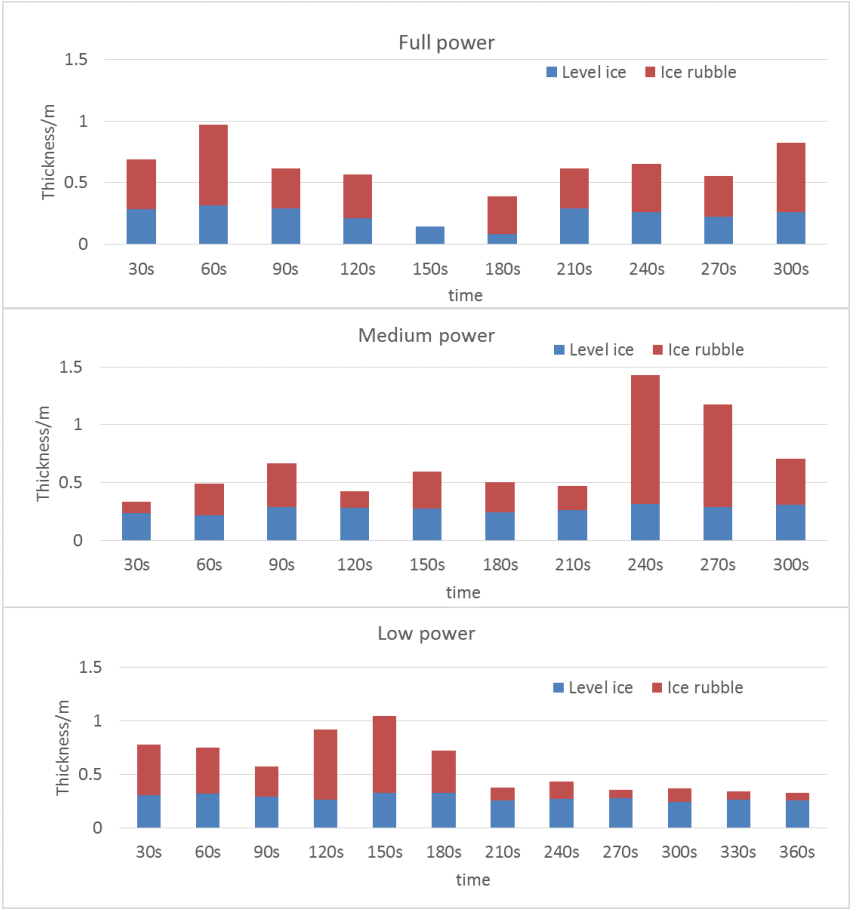

Figure 12: 30 seconds average thickness

full power, medium power and low power. The figures show that the powers are fluctuating around these set values. Specifically, full power have a relatively large variation range, from 3000kW to 6000kW. Medium power is approximately constant before the last 1.5 minutes when there appears a sudden drop to 1600kW. Low power does not change significantly for the whole six minutes. Combining speed, power and ice thickness data, it is found that the first 3.5 minutes of medium power case is the most stable part in terms of power, speed and ice thickness. The difference between EM and stereo camera measured thickness is also less significant compared to most of the other parts. This makes it convenient for the comparison between simulation results and full scale data.

Figure 14 presents the time history of speed during the test. With full power, the speed varies between 2 and 6 m/s, while with medium power 1 to 3 m/s and low power 1 to 2.5 m/s. It is noticed that each time history of speed has experienced significant drops, which may be due to power or ice thickness change.

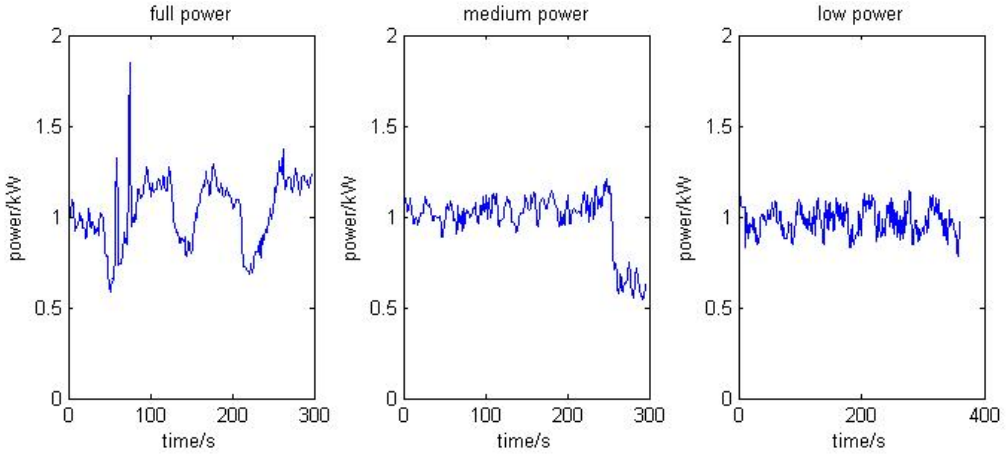

Figure 13: Power output scaled by set power

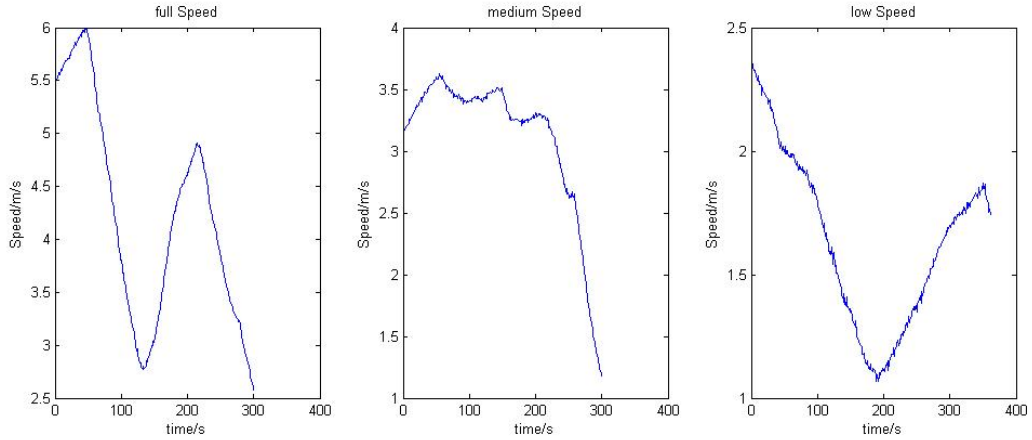

Figure 14: Ship speed in ice

4.3 Resistance calculation

Accelerations of the ship at each second can be calculated from the speed data. To make a comparison with simulated ship resistance, it is useful to find the real resistance based on available data. Considering x-direction forces, there is the following relationship in scalar

$$ma = T_{net} - R_i \tag{61}$$

where T_{net} is the net thrust, R_i is ice resistance, m is ship mass. Net thrust can be calculated by equation 40. Ship mass is known from DNV database (vesselregister.dnvgl.com/VesselRegister/vesseldetails.html?vesselid=30528) and acceleration can be calculated from speed data. Then ice breaking resistance is obtained. It should be noticed that the weight can vary with different loading cases. Since the loading condition of this ship during ice trial is not known, weight deviation can be a possible error source. With less load, the calculated resistance will be higher when accelerating and lower when decelerating. Figure 15 shows calculated total

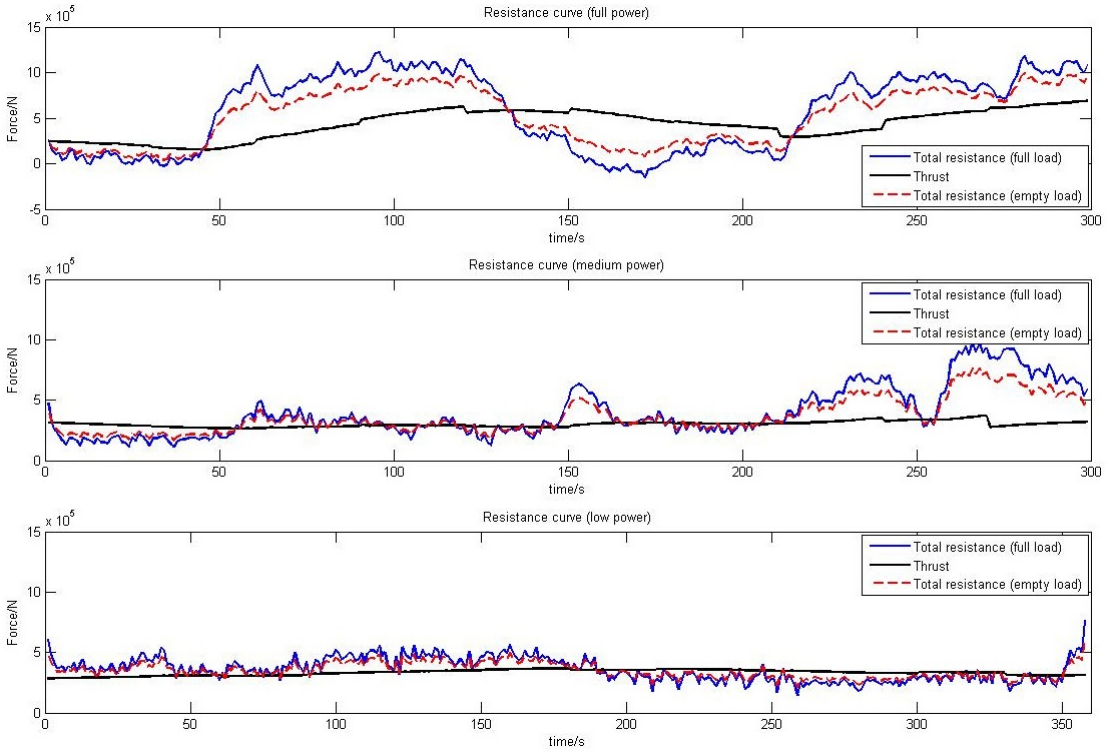

Figure 15: Time histories of resistance calculated from data assuming full load and empty load

ice forces varying with time under two loading conditions: full load (blue real line) and empty load (red dashed line). The black real line is ship thrust calculated by net thrust model. From the figure it is seen that the difference in time histories of resistance with different loading condition is actually small (mostly below 10% difference). Therefore, in this thesis full loading is assumed with a total ship mass of 13687t.

Actually, the calculated resistance is not 'real resistance' because it includes the possible error from net thrust model, which should be kept in mind when doing the comparison. One thing is seen strange in full power case that the resistance during 0s to 50s and 150s to 200s are very close to zero. Actually, from further calculation, ice resistance during 0s to 50s is even less than calculated submersion force, which results in a plus value for ice breaking resistance. This is obviously not true. Since ship speed and power data are not likely to be wrong, there is a possible reason that there exists a 'phase difference' between ice thickness data and power or speed data. Assume ice measurement device is installed at ship bow area. It takes some time before the ship body aft of bow encounters the ice with measured thickness. If the ship was sailing in a thin ice field before 0s, it is possible to have calculated resistance. The reason why this phase difference is not seen in other power cases is that the ice thickness varies much less significantly in medium and low power cases, which make it insensitive to this possible phase difference.

5 Pre-discussions on the simulation model

Now the simulation method and full scale data are introduced in detail. Prior to the simulation, a preliminary discussion regarding the model is conducted to identify the influencing factors of the simulation and set up a clear criteria for evaluation. In section 5.1, icebreaking process is qualitatively analysed within an icebreaking cycle. Loading rate, bending bearing capacity and broken cusp size are identified as influential factors on the accuracy of the model. This analysis provides theoretical input to the quantitative discussion in chapter 8 and will be verified by simulated results. Section 5.2 sets up an criteria for the evaluation work, which gives priority on the importance of comparison objects. Resistance is identified as the most essential index to justify the simulation and time history of speed follows.

5.1 Analysis of icebreaking process

Ice breaking at a fixed point on the ship can be regarded approximately as a periodic process, starting from contacting with ice sheet and ending at contacting the next ice. Ice breaking along the whole ship is then a superposition of all the periodic forces along waterline. From a qualitative analysis, the influence of implemented modifications can be identified theoretically.

Figure 16 is a sketch made by the author to describe a typical icebreaking period, which is commonly used by researchers to represent ice breaking process. The numbers in this figure are just used as a relative value, so magnitude does not matter. Assuming a ship is moving through the ice with constant speed v. At a particular point along the waterline, Submersion force is seen as constant with a magnitude of 5N. With original model (blue line without marker), ice breaking force starts to increase by 2N per second with the contact area increasing. Ice is broken at 5th second when the force exceeds its bearing capacity, which is 10N in this case. After that, breaking force disappears and only submersion force is left, until the ship contacts another ice wedge at the end of this period (10th second). The length of a period is decided by the breaking radius and ship velocity, which determine the distance and time between two successive contacts with ice. According to equation 25, ice breaking radius is only dependent on characteristic length and ship velocity, non-related to breaking force. Therefore, the period is constant for a certain velocity as long as the breaking radius model remains unchanged. So the influence of the modifications to the model can be analysed within one period.

The average resistance within a period is derived by dividing the integration of area under resistance curve by period time. Three factors can be identified influential to average resistance, which are loading rate, bearing capacity and broken cusp size. Loading rate decides loading time. Bearing capacity determines top force value. Broken cusp size, which is the breaking radius in this model, divided by velocity gives period time.

Non-linear p-a relationship and area modification affect loading rate. As will be discussed in figure 18, the non-linear p-a relationship implemented here leads to a higher loading rate, which, as illustrated in figure 16 (thin purple line with

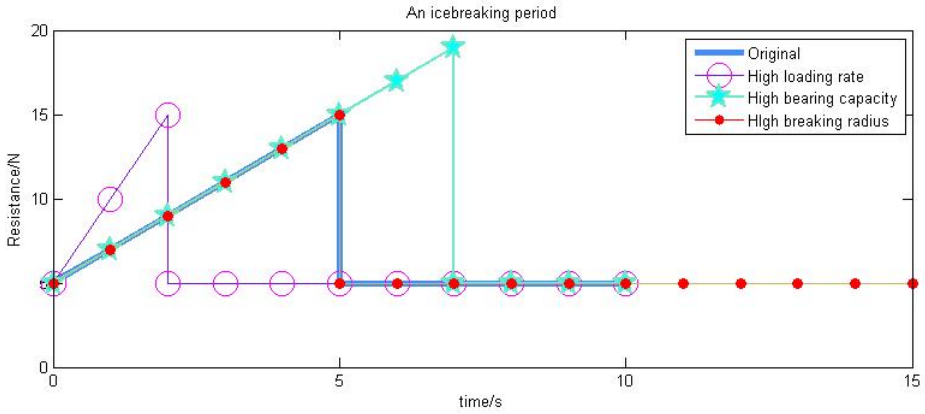

Figure 16: Icebreaking force evolution within a typical period

circle), shorten the ice breaking time and decrease average resistance. Oppositely, the area modification reduces the contacting force under same area, which gives a lower loading rate and thus a higher average resistance.

Bending bearing capacity determines how large the force can be before ice broken. According to figure 24, with a dynamic bearing capacity model, the bearing capacity decreases at low velocity and increases at high velocity. According to the light blue line with five-pointed stars in figure 16, a higher bearing capacity could lead to a larger resistance and vice versa. Thus dynamic bearing results in more resistance with high speed and lower resistance with low speed. Besides dynamic bearing capacity model, the empirical coefficient C_f also affects the simulation results by the same mode.

The third type differs from the other two by changing the period. A random breaking radius and the coefficient C_l and C_v can make this change by altering breaking radius. The effect is shown in light yellow line with red dots in figure 16. A larger radius contributes to a longer period and thus leads to less average resistance within one period. From this it is deduced that the distribution of random breaking radius is important in the magnitude of resistance. The more larger values it produces, the less resistance there will be.

5.2 Evaluation criteria

It is very important to really understand what it means by 'evaluation'. Since this thesis looks into the performance of a model under varying power and ice thickness, which is quite different from the validation part in former articles but much more close to reality, it really matters to find a criteria to evaluate the model in a decent, and comprehensive perspective. Naturally, there can be at lease three criteria for evaluation, which are resistance, time history of speed and distance sailed.

Resistance is a direct output from the simulation. It concerns how much loads the ship will endure and how much power it will consume for a certain mission. It is definitely required to be included. Velocity tells how fast the ship can run under certain power and ice thickness. It tells more about what is happening for a certain

moment. A good time history of speed can convince people of the usability of the model. Distance, which divided by time gives average velocity, is an important index in commercial calculation when people use it to evaluated the time consumption or how many passages a ship can run for a certain time.

Now assume there is a deviation between simulated resistance and real resistance at time t_1 to t_2 and then back to normal. This deviation in resistance will lead to a constant deviation in velocity and an growing deviation in distance from t_2. In other words, velocity deviation is the integral of resistance deviation and distance deviation is the integral of velocity deviation. If a deviation in resistance occurs in early time, it will have more influence on time history of speed as well as average speed than a later one. This implies that resistance comparison is more trustworthy than the other indices. However, since measuring ice resistance is really difficult, the resistance used for comparison has to be calculated from full scale data, which inevitably introduces some error sources during calculation.

However, velocity and resistance as well as thrust are coupled with each other. A good model can eliminate the velocity deviation gradually by balancing thrust and resistant. Besides, there are some cases with similar resistance but quite different velocities. Thus time history of speed should be regarded as another factor when comparing the resistance. A best simulation is one that gives similar resistance values as well as time history of speed and average velocity. If that does not happen, a similar resistance value and decent time history of speed is more preferred rather than average velocity.

When comparing results, considering there are certain error sources within the model, a deviation of below 10% is defined as good and below 20% is acceptable. If simulation gives a difference larger than 20%, it is considered too large thus the usability is doubtful.

6 Simulation of S.A. Agulhas II

In this section, the motion of S.A. Agulhas II is simulated by both the numerical method and empirical methods. Empirical coefficients are selected according to previous works done by other researchers. Alternative modifications are implemented into the numerical method.

6.1 S.A. Agulhas II

S.A. Agulhas II is a South African icebreaking polar supply and research ship which was built in 2012. It is powered by four six-cylinder Wärtsilä 6L32 medium-speed diesel generating sets, each producing 3,000 kW (4,000 hp). The ship has a diesel-electric powertrain with two Converteam 4,500 kW propulsion motors driving 4.5-metre (15 ft) KaMeWa controllable pitch propellers, a relatively uncommon feature in diesel-electric ships which usually utilise fixed-pitch propellers. (en.wikipedia.org/wiki/S._A._Agulhas_II) The main dimensions of the ship is listed in table 4.

Table 4: Dimensions of S.A. Agulhas

Dimension	Symbol	Value
Length overall	L_{oa}	133.4m
Length of water line	L_{wl}	123.28m
Breadth	B	22m
Draught	d	7.62m
Propeller diameter	D_p	4.5m
Service speed	v	14knots
Displacement	Δ	13687t
Waterline opening angle	α	33°
Flare angle at bow	Φ	27°
Hull normal angle at bow	Ψ	42°
Mass moment of inertia about z-axis	I_z	$1.77 \times 10^{10}\ kgm^5$

An important feature of S.A. Agulhas II regarding hull form is that the parallel ship part is purely vertical (flare angle 90 degrees). This has large influence in resistance and will be discussed in later sections.

Full-scale measurements were performed on S.A. Agulhas II during ice-trials in the Baltic Sea in 2012. Ice loads on the ship hull and propulsion system were measured concurrently with ice-thickness and whole-body vibration comfort for controlled maneuvers in a level ice field. (Bekker et al. 2014) The ice thickness is measured by visual observation, a stereo camera and an EM device. These data are utilised in this thesis for evaluation use.

6.2 Simulation by the numerical method

6.2.1 Selection of empirical parameters

Selection of C_f Tan et al. (2014) did a literature study which revealed a big scatter of C_f values in former works. From his study, different authors use varying C_f which can be as low as 1.04 and as large as 4.1. The scatter implies that the numerical adjustment of C_f was made to agree with either full-scale measurement, or with empirical resistance formulae. (Tan et al. 2014) It is noticed that for ship-ice contact, which has a larger velocity compared to platform-ice contact, a high coefficient is more often used. Thus C_f is set to be 3.2 in this thesis.

Selection of C_l C_l is very important in determining the breaking radius, which has a big influence on resistance. Thus it should be selected carefully in practical use. Wang (2001) set C_l to be 0.32 in her simulation. Su (2011) then used 0.30 and 0.27 in his PhD thesis. According to Kuuliala (2015), based on the results from Enkvist (1972), an R/l_c ratio of 0.3-0.7 is typical seen in full scale test. From some preliminary trials, it is found by the author that a C_l value of 0.4 gives a reasonable results.

Selection of C_v Kuuliala (2015) investigated the sensitivity on C_v in a range of [-0.12, -0.08]. Resistance appears not very sensitive on the selection of C_v. According to figure 15, ship resistance shows certain positive correlation to ship speed. For more dependency on velocity, C_v here is selected to be -0.12.

6.2.2 Other inputs and settings

Table 5 lists relevant parameters regarding ice properties. σ_c and σ_f are set according to Bekker et al. (2014) from tests onboard. The others are consistent with those adopted by Kuuliala (2015).

Table 5: Ice properties

σ_c	1.5 MPa
σ_f	0.433 MPa
E	8 GPa
μ	0.15
ν	0.33
ρ	1020 kg/m^3
ρ_i	900 kg/m^3

As aforementioned, stereo camera measured ice thickness data and ship power data are stable, with insignificant fluctuations. Thus they are averaged every 30 seconds for easy implementation in this simulation. In other words, the ice thickness and power is set constant within every 30 seconds, as shown in figure 17. EM measured ice thickness is used for determining ice rubble thickness. Since it fluctuates quickly,

these thickness data are averaged with 5 seconds interval, by which the variation of ice thickness becomes regular. Initial velocities of the three power sets are read from the speed figure, which are 5.49, 3.18, and 2.37 m/s for full, medium and low power respectively.

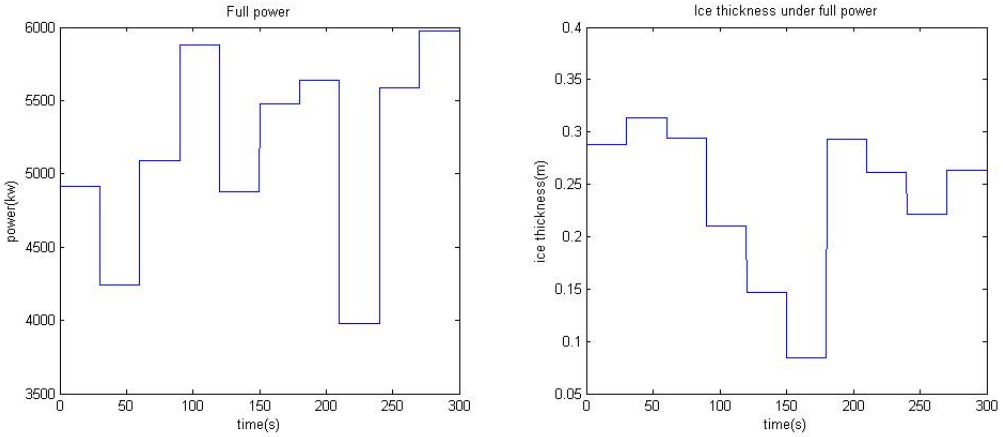

Figure 17: 30 seconds averaged power and ice thickness

For each power set, cases by original model and with different combinations of modifications (p-a relationship, dynamic bending capacity and random breaking radius) are run by the codes. Velocities, motions, forces and breaking patterns are recorded as the output. Table 6 listed the cases that have been run. 1 means with this modification while 0 means without. In power column, h means full power, m means medium power and l means low power.

Table 6: Test matrix

Test No.	power	random R	rubble res.	p-a	dynamic bending	C_l
1−3	h/m/l	0	0	0	0	0.4
4−6	h/m/l	1	0	0	0	0.4
7−9	h/m/l	1	0	1	0	0.4
10−12	h/m/l	1	0	0	1	0.4
13−15	h/m/l	1	1	0	0	0.4
16−18	h/m/l	1	1	1	0	0.4
19−21	h/m/l	1	1	0	1	0.4
22−24	m	1	1	0	0	0.4/0.5/0.6

6.3 Alternative modifications

Non-linear p-a relationship The non-linear pressure-area relationship model implemented here is that used by Kuuliala (2015). As shown in figure 18, this model gives a larger contact force in the area range of [0,1], where most contact areas are located. There are many other p-a models which use the same form but with different

coefficients. This model is used as a representative for the discussion of the influence of p-a relationship.

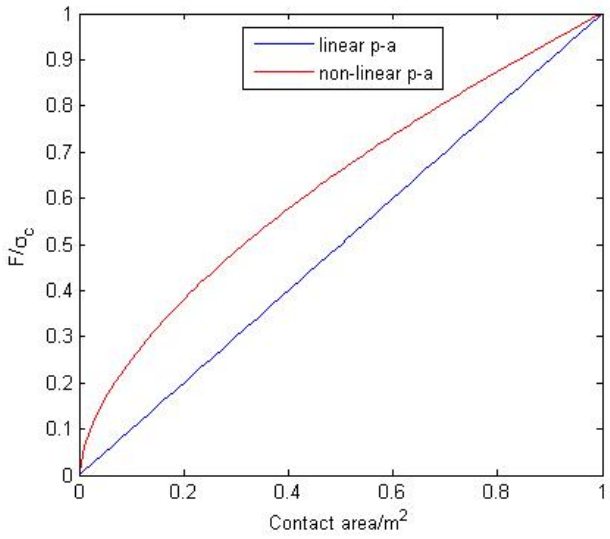

Figure 18: Comparison between linear and non-linear p-a relationship

Dynamic bearing capacity model The model is given in equation 24. A speed dependence instead of an empirical coefficient is incorporated here. The relationship is derived by dimensional methods. Figure 24 illustrates a magnitude comparison between the original and modified model with changing speed. Since the difference in expressions is the coefficient, which is C_f in static method and $1.65 + 2.47v_2^{0.4}$ in dynamic method. The figure compares the difference between these coefficients.

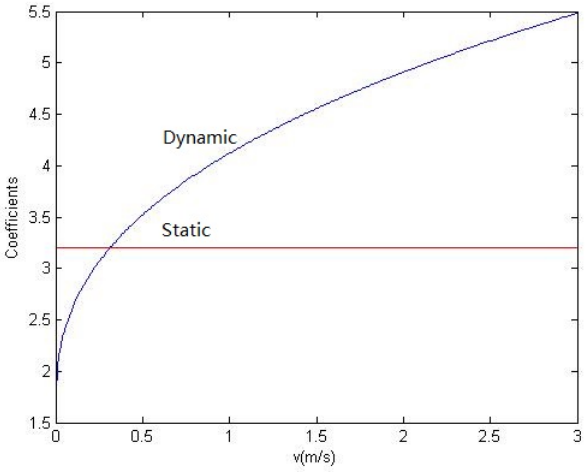

Figure 19: Comparison between static and dynamic bending models

Note that this v in the figure is not ship speed. Instead, it refers to the relative normal velocity of the contact plane, which is usually much less than ship speed. It

is demonstrated that the dynamic model gives a higher bearing capacity when v_2 is greater than 0.312 m/s.

Random breaking radius Breaking radius is randomly generated with a mean value of calculated breaking radius and a standard deviation of 0.287R. However, in order to avoid abnormally large or small values, a lower and upper radius limitation is used as a restriction. The breaking radius is limited between $0.1l_c$ and $2l_c$, where l_c is the characteristic length.

Contact area modification As stated in section 3.3.1, contact areas are modified according to Zhou et al. (2016). Since the ice sheet is suppressed by the ship, contact areas are reduced, which gives less contact force. This model should be implemented into the method by iteration. However, the computation proves to be very time consuming when the author tries to apply this model. Due to limited time, this modification is only qualitatively discussed instead of numerically simulated.

6.4 Simulation with empirical formulas

The empirical formulas derived by Lindqvist (1989) and Riska et al. (1997) are two widely used empirical formulas for estimating level ice breaking resistance. In this thesis, the motion of S.A. Agulhas is also simulated by theses methods as a comparison to that by numerical methods to find advantages and shortages in using numerical method.

The simulation process is done by several steps. Firstly, ice thickness and power output are averaged into 30 seconds values, which is same to numerical simulation. Then the motion is simulated in one DOF. The time is divided into 0.001 seconds intervals. This time interval proves to be accurate and fast enough by simulation. At each time step, forces due to propulsion and ice resistance are calculated and then acceleration is achieved, which determines the motion of the next time step. Simulation is then done step-by-step. The output resistance is separated into submersion force and icebreaking force for Lindqvist's formula and into bow resistance and parallel part resistance for Riska's formula, in order to compare the results in detail.

7 Results

In this chapter, simulation results from both numerical method and empirical formulas are presented. In section 7.1, numerical simulations are carried out in 0.001s time steps under full, medium and low power. For each power set, results with implemented modifications are given separately. The results are introduced by velocities and motions, forces and ice breaking pattern. Resistance and velocities are compared with full scale data while breaking pattern is shown for discussion. In section 7.2, simulation results done by Lindqvist's and Riska's formula are presented. Resistance and velocity are plotted according to the output.

In this section, abbreviations listed in table 7 are used in figures and tables for simplicity.

Table 7: Abbreviations in this chapter

Ori	original Su's model
Rub	model with rubble resistance considered
Ran	model with random breaking radius
Dyn	model with dynamic bearing capacity
Non	model with non-linear p-a relationship
Are	model with area modification
ave	average

7.1 Simulation results by numerical methods

Numerical simulation gives results of 24 cases in total for all three power sets with speeds, forces as well as ice breaking patterns. It really matters to organise them in order. In following subsections, the results from the original model is presented first, followed by results with modifications. Results are grouped by time history of speed, time history of ice resistance and breaking pattern. After all results by numerical simulation are presented, a summary is conducted to collect useful information together. Besides these, a short sensitivity study regarding C_l is conducted since it concerns much about breaking pattern. The presenting of results follow the investigation process by the author. Firstly problem is identified and then solutions are proposed, tested and commented.

7.1.1 Original Su's model

Figure 20 shows the time history of speed from original simulation model (blue dashed line) under three power sets, with the real speed (red real line) as a reference. It seems that there is a significant difference in simulated results and real data, especially under full and medium power. The curve under full power generally shows a similar varying trend with measured results, except for last minute, where it goes up to 5.1 m/s instead of dropping down. Time history of speed under medium power

behaves strange. There is an unexpected sudden drop in speed at 100s to 150s under medium power, while in measured results it goes quite smoothly. However, time history of speed of low power case fits the reality quite well. The speed bottoms at 200 s with an value of 1 m/s and finally ends with 1.8 m/s, which is quite close to measured results. Despite of the difference in curve trends and values, the average velocities simulated by original model are not far from real case, which are 4.73, 2.76 and 1.76 m/s while full scale data give 4.22, 3.10, 1.63 m/s. The deviations are around 10%, which looks quite acceptable in accuracy.

To find the reason of the dissimilarities in time histories of speed, time histories of ice breaking resistance under three power sets are plotted in figure 21. The grey lines are raw simulated ice breaking forces in 0.001s interval while the red lines plots 5 seconds averaged forces. It is found from the figure that time history of force can be categorised into two types, one with regular shape and similar peak values (generally around 1×10^5N), for example last 100 seconds with full power, and the other with huge values (as high as 2×10^6N) and irregular variations, for example around 70th second with full power. This looks abnormal that the force has such significant changes while the ice thickness actually varies very slightly. Combining speed and force curves together, it is seen that the sudden change in speed curve under medium power corresponds to large force values during 100s to 150s. This correspondence is also seen with other power sets. For example with full power during 60s to 90s and low power around 200s, there are also significant speed drop with large ice forces.

The average resistance with full, medium and low power sets respectively are 395, 362, 343 kN, while the real case gives 567, 391, 355 kN. The deviation is 30% for full power case and around 10% for medium and low power cases.

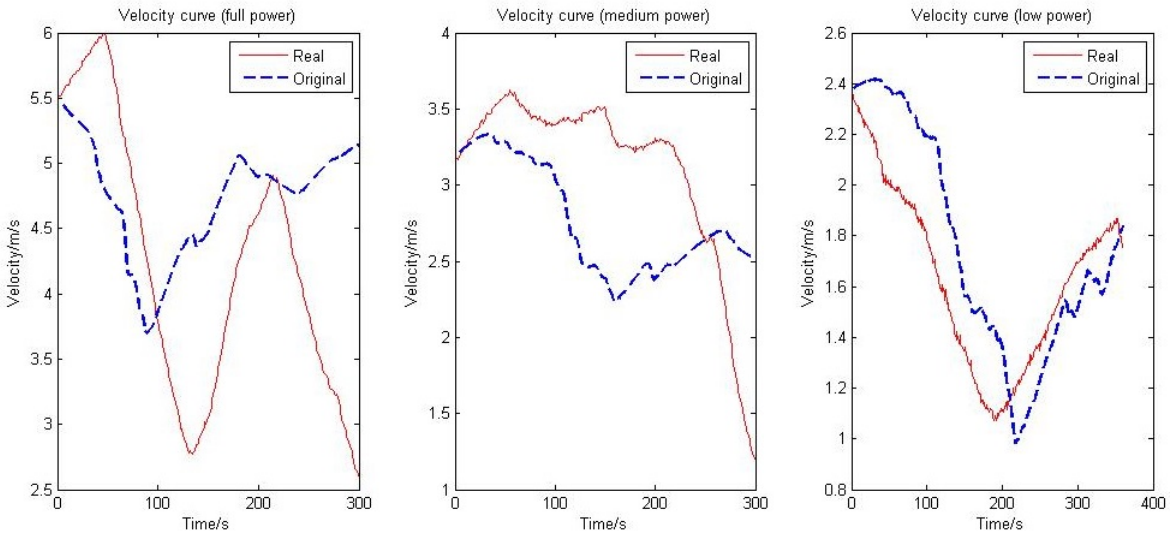

Figure 20: time history of speed by Su's model

Breaking pattern is then examined to figure out why there are huge force changes while ice thickness varies just slightly. The ice sheet around ship hull is drawn at two specific time under full power: 70s when there is huge force and 240s when force

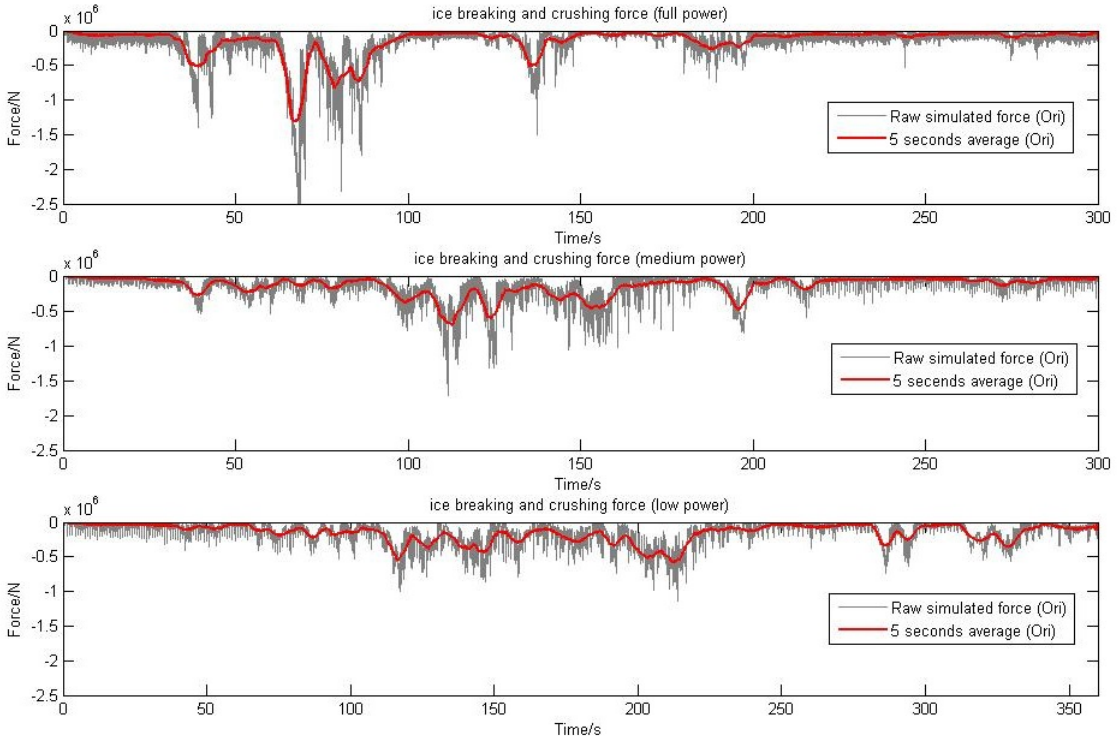

Figure 21: Time history of ice crushing and breaking forces by Su's model

goes smoothly. As drawn in figure 22, the ice channel created by the ship is very narrow at 70s compared to that at 240s, with almost the same width as ship breadth. As a result, there are very large contact area between ship and ice, as shown in the red rectangular. Since ship has sway and yaw motion, there could be large crushing forces from these contact areas, which finally leads to significant friction as resistance. Thereby the sudden speed drop and large ice forces can be explained. This narrow channel and large contact area phenomenon is referred to as shoulder crushing by Su (2011).

This examination of breaking pattern gives an indication that the good fit of time history of speed with low power may be just a coincidence. To further prove this, figure 23 plots some time histories of speed under low power with non-linear relationship and dynamic bearing capacity implemented. It can be seen that the curves are quite irregular, giving very different velocity predictions. For example, with non-linear p-a relationship model implemented, ship speed firstly goes level with value of 2.4 m/s, then bottoms at around 250s with 2.1 m/s and finally goes up to 2.4 m/s. The drop of speed is again significantly influenced by when shoulder crushing happens. Since non-linear p-a relationship and dynamic bearing capacity do not lead to any difference in breaking pattern, the conclusion can be drawn that the output of the model has large fluctuation which depends largely on shoulder crushing.

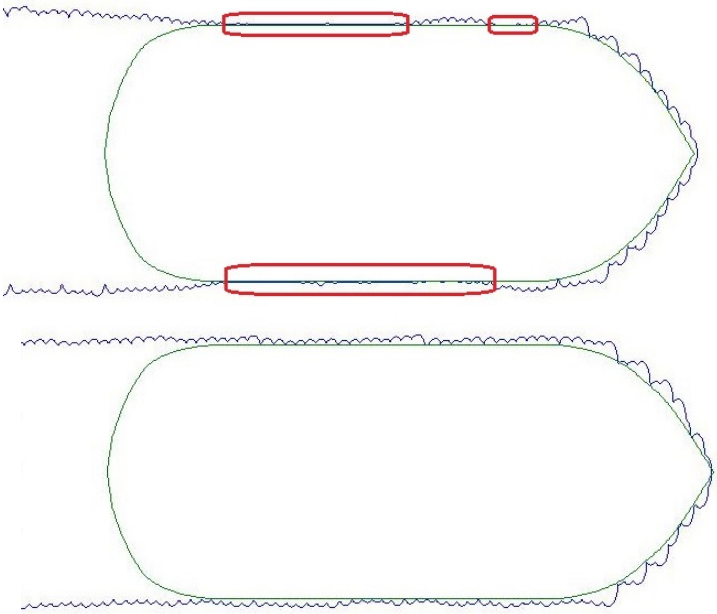

Figure 22: Ice sheet pattern around ship waterline at 70s (upper) and 240s (lower) with full power

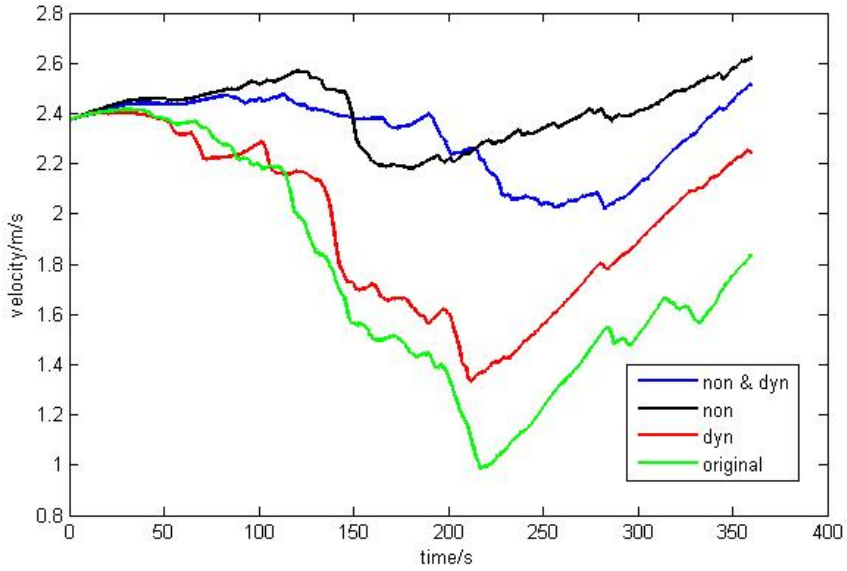

Figure 23: Time history of speed with non-linear p-a relationship and dynamic bearing capacity under low power

7.1.2 Random breaking radius model

Figure 24 gives the time history of speed from simulations with random floe radius model implemented (blue dashed line), with results from original model (black real line) and from measured data (red real line) shown as reference. Under full power, the

time history of speed is generally above measured results except for the first minute. Bottom speed (4.3 m/s) is not as low as given by original model (3.7 m/s), which is already beyond real speed (2.8 m/s). There exists an improvement in time history of speed under medium power, where the velocity changes smoothly between 100s to 200s, which is more like measured results. Unlike measured data, simulation results fail to predict the significant drop existing during last 1.5 minutes. It ends by 2.5 m/s while measured data by 1.2 m/s. The speed under low power case becomes larger than that in original model, bottoming by 1.8 m/s and ends 2.2 m/s. Compared to original model, the problem of abnormal sudden speed change is not seen here with randomness introduced. The average velocities of simulation with random model are 4.84, 3.01 and 2.05 m/s, which gives 15%, -3% and 26% deviation compared to measured results.

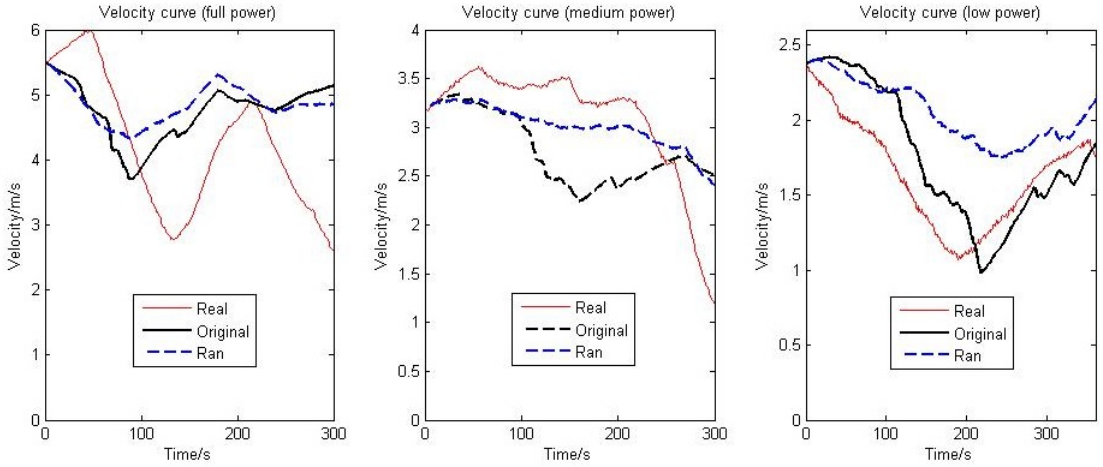

Figure 24: Time history of speed with random floe radius

As mentioned in section 4.2, power, speed and ice thickness are quite stable and ice rubble is not significant during 0 to 210s with medium power. Therefore, it is very suitable to evaluate the capacity of this model for giving speed and resistance prediction. Average simulated speed during this time period is 3.12 m/s while average real speed is 3.40 m/s. The difference is below 10% so the prediction is actually quite good.

Figure 25 illustrates the ice breaking forces with random breaking radius implemented, with that by original model as reference (blue dashed lines). The grey lines are raw simulated forces in 0.001s interval while the red lines plots 5 seconds averaged forces. Compared to the results by original Su's model, time history of forces with random breaking radius are more regular here, with seldom dramatic increase or decrease. Forces are mostly below 500 kN while from original model it can be as high as 2500 kN (figure 21). The average resistance including submersion force are 394, 346, 314 kN under full, medium and low power respectively, which similarly gives a deviation of 30% for full power case and below 10% for medium and low power cases. The average resistance are close to those by original model. This indicates that with random breaking radius model, the huge peak forces which

occur with original model are smoothly distributed along the whole time field. For example, in full power case, there are no high peak values around 70th second with random breaking radius, The resistance is then higher than that of original model during last 100 seconds. For this reason, the average resistance for whole 5 minutes just has 1 kN difference between them.

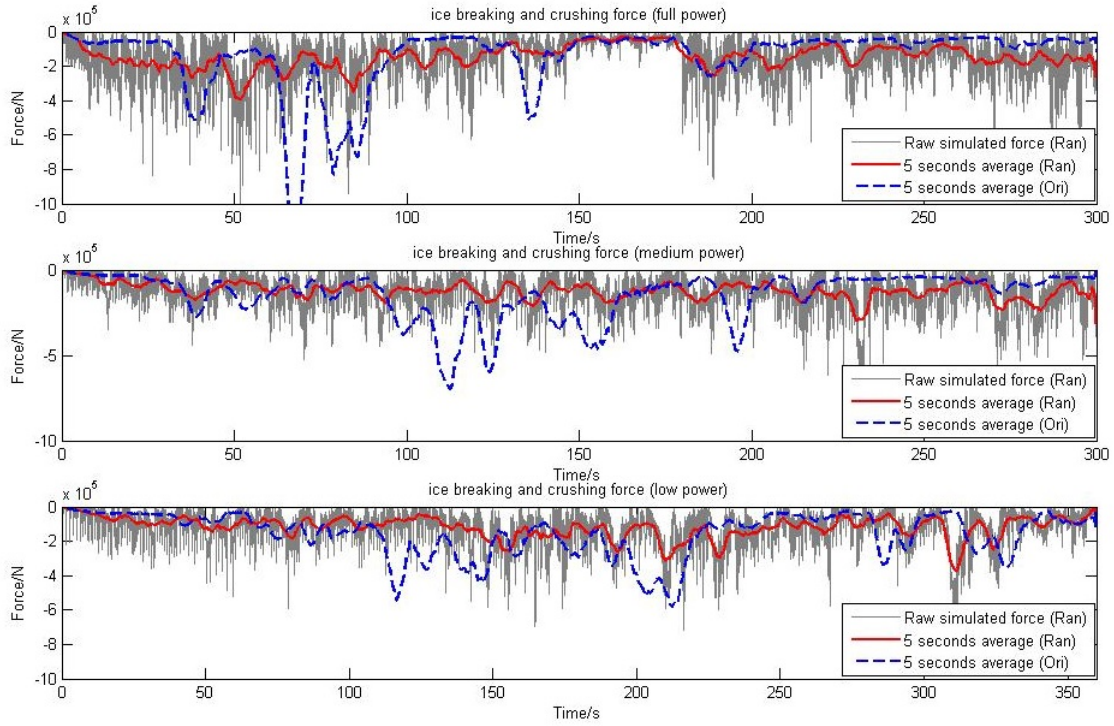

Figure 25: Time history of ice crushing and breaking forces with random floe radius

Again, ice sheet pattern is examined to find the reason why the unexpected sudden speed drop and force change are eliminated with this randomness applied. The ice sheet pattern at 300s with medium power is plotted in figure 7.1.2. Compared to those in figure 22, the ice edge around ship waterline in this figure is more irregular in shape, with no significant shoulder crushing. The contact area is slightly larger than the lower one in figure 22. This ice sheet pattern is witnessed almost the whole time period. This well explains the difference in force and speed curves. With this randomness, the unexpected sudden speed and force changes are well eliminated, which is good not only for practical use, but also for more convincing conclusions from further research in this thesis. It is interesting that the output now has more certainty with a randomness model applied. Due to this reason, in following text, other modifications are implemented always together with this random breaking radius model.

Figure 27 shows a box plot of ice floe radius under low power, one by deterministic breaking radius and one with random. The red lines in the boxes are the median values of breaking radius while the value range in the boxes takes up 50% of all data. It tells that ice floe radius are more diverse with random floe size model which at the

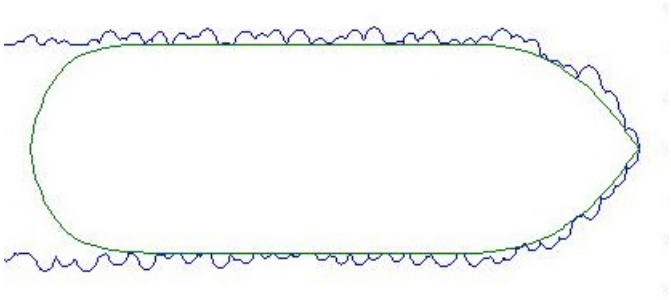

Figure 26: Ice sheet pattern around ship waterline at 300s with medium power

same time gives a slightly lower median value. Radius of ice floes are mostly below 3 meters, which is in a decent range considering the reality.

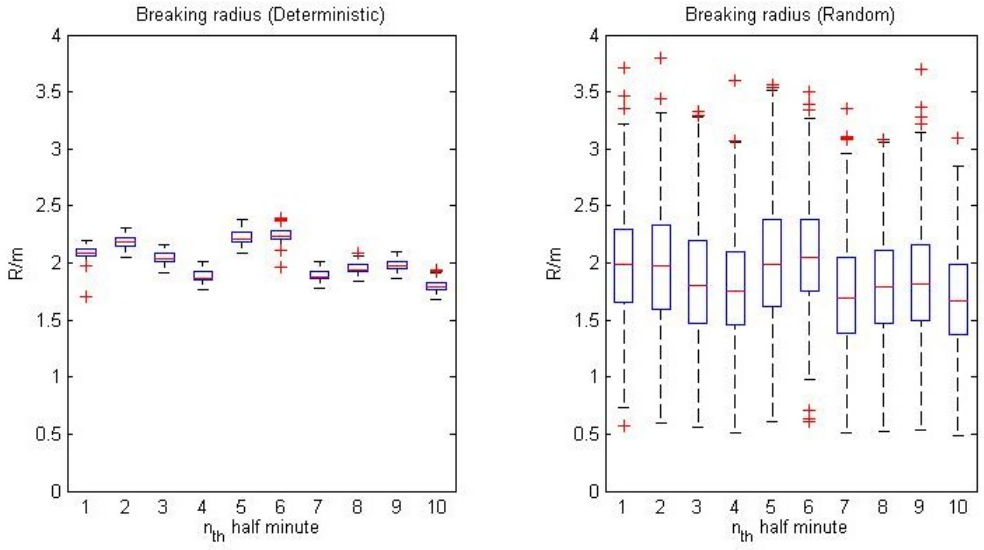

Figure 27: Boxplot of ice floe radius with deterministic (left) and random (right) breaking radius

As a short conclusion, random breaking radius helps to get rid of unexpected speed and force change. But the deviations in average speed and resistance are still large in certain cases. The difference in speed values are quite small during 0s to 210s with medium power, but very obvious in other time with all three power sets.

7.1.3 Ice rubble resistance

Figure 24 gives the information that simulation usually underestimates the resistance when there is significant speed drops in real time history of speed, for example during last 1.5 minutes with medium power and the first 190 seconds with low power. Going back to figure 15, it is seen that within these time period, there is obvious difference between EM and stereo camera measured ice thickness. Therefore, a ridge resistance

formula (equation 36) is applied to take account of this resistance source. Figure 28 plots the time history of speed when rubble resistance is included (green dashed line). The time history of speed without rubble resistance accounted is plotted in blue dashed line as reference and real speed is plotted in red. As shown in this figure, simulated ship speed is greatly reduced. Bottom speed under full power reached 3.9 m/s and it does not rise in the last minute any more. With medium power, the speed shows a larger difference with measured data during first 3.5 minutes with average speed of 2.66 m/s (-22% difference), but finally follows a significant drop till 0.9 m/s at the end, which is not seen without rubble resistance considered. With low power, speed drop before its bottom is now much more significant. The bottom speed is 0.6 m/s at 180s and final speed at 360s is 1.7 m/s, which is close to measured data. With rubble resistance, average speeds become 4.43, 2.26 and 1.27 m/s, with relative values of 5%, -27% and 22%.

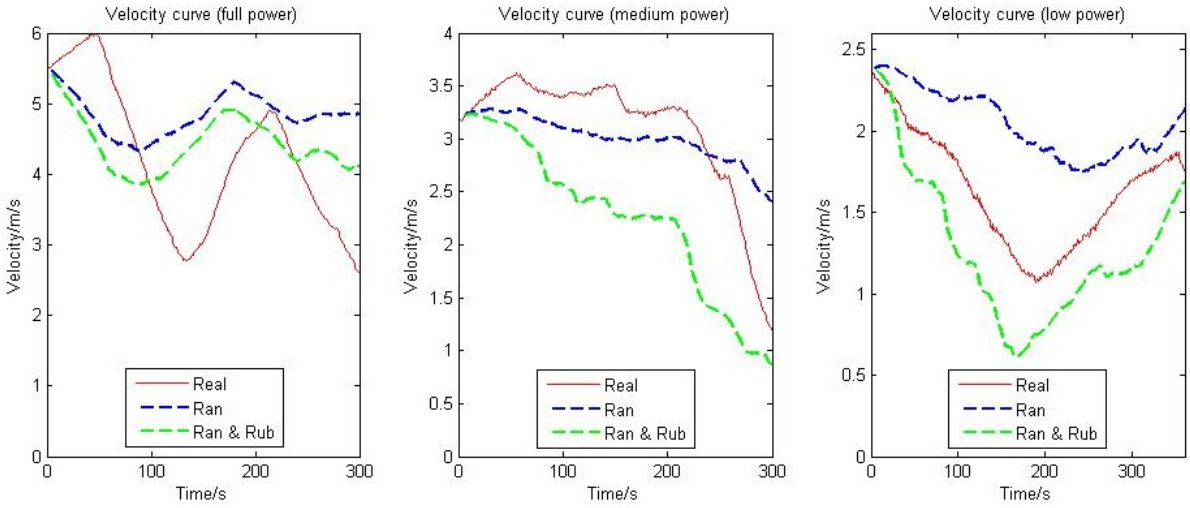

Figure 28: Time history of speed with rubble resistance accounted

Figure 29 plots simulated ship resistance due to ice rubble, together with time history of rubble thickness. Since models with dynamic bending or non-linear p-a produce similar resistance curves, here only the result by the model with random breaking radius is presented. It shows a linear dependence of resistance on rubble thickness. Resistance can be as large as 600 kN when there is a peak value (1.3m) of rubble thickness. Since simulated average resistance due to level ice breaking and underwater part is about 300 to 400 kN, ice rubble takes up a significant portion of total resistance.

Time history of total resistance is plotted in figure 30. From this figure, simulated resistance agrees with calculated resistance best with low power, acceptable with medium power and not very good with full power. The average resistance values are 483, 475 and 378 kN, giving a relative difference of -15%, 21% and 6% with calculated resistance.

Figure 31 and 32 are plotted here in order to have a better view of the influence of ice rubble on resistance evolution. They are simulated only with random breaking

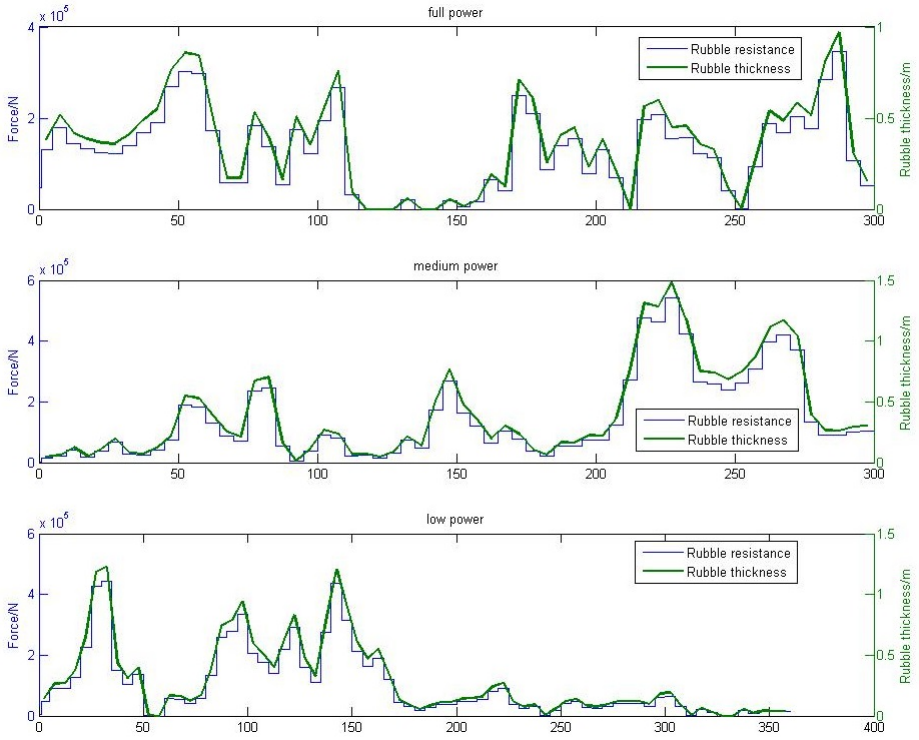

Figure 29: Time history of resistance due to ice rubble and ice rubble thickness

radius model. Figure 31 illustrates the accumulative resistance which is derived from the integral of resistance over time. The red line is calculated resistance from full scale data. Green and blue lines are simulated resistance with and without rubble considered. Figure 32 plots the average resistance within every 30 seconds. Line colours are defined same to figure 31. This figure gives more information on resistance evolution while figure 31 tells more about values. With rubble considered, resistance values are closer to full scale data with full and low power but farther with medium power. The evolution of resistance is obviously improved with rubble resistance taken into consideration. In figure 32, with medium power, simulated resistance without rubble considered goes almost level, while with rubble resistance, there is an significant increase at 8th half minute, which is very similar to the resistance increase of full scale data during last three half minutes. With low power, resistance is obviously higher during first 5 half minutes than the rest time with rubble considered, which is very consistent with full scale data.

Figure 32 also gives a good perspective to examine the aforementioned 'phase difference' between thickness data and power or speed data. With full power, ice thickness is obviously smaller during 120s to 180s than other time, which is most likely to result in smallest resistance. It is seen that the resistance curve calculated from real data bottoms at 6th and 7th half minutes while simulated resistance with rubble accounted bottoms at 5th and 6th. There is a phase difference of around 30 seconds. The green line can fit the red better if it is moved to the right by 30 seconds. With medium power, the maximum ice thickness occurs at 8th and 9th half minutes.

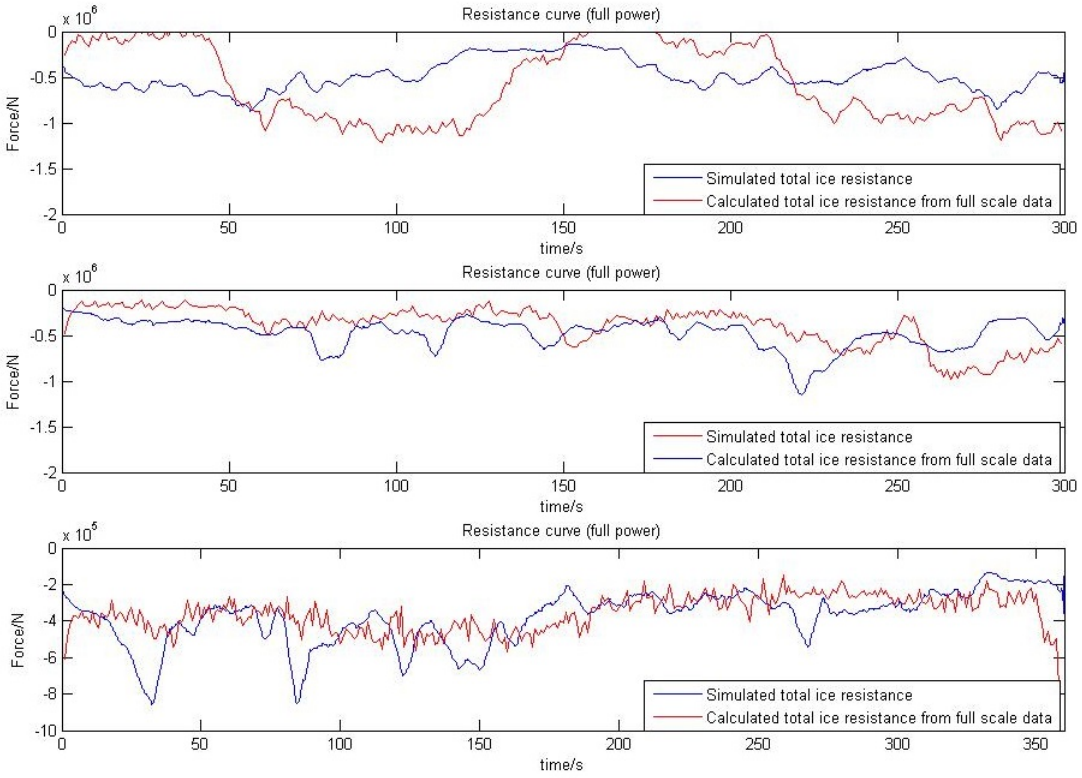

Figure 30: Time history of total ice resistance including rubble resistance

Calculated resistance peaks at 9th and 10th half minutes while simulated resistance at 8th and 9th. There is again a phase difference around 30 seconds. Besides, there is a thickness drop during last half minute. This drop is not reflected in calculated resistance since the data end there. With low power, ice thickness between starts to drop from 5th half minutes. This drop results in a decrease in resistance, which is seen at 5th half minute by simulated resistance and 6th half minute by calculated resistance from full scale data. This again tells the possibility of the presence of phase difference.

7.1.4 Dynamic bearing capacity and non-linear p-a relationship

Time history of speed with dynamic bearing capacity (blue and green dashed lines) are plotted in figure 33, with results from model with only random breaking radius (black and orange real lines) as reference. The green dashed line and orange real line are those with rubble resistance accounted. The trends and values does not change much with dynamic bending model. With full power, speeds are slightly below the result with static bending capacity while speeds are a little above it with medium and low power. More specifically, it seems that predicted resistance increase with high speed and decrease with low speed. Average velocities under three power sets are 4.79, 2.99 and 1.93 m/s without rubble resistance, which gives 14%, -4% and 18% difference compared to reality. With rubble resistance considered, average speeds

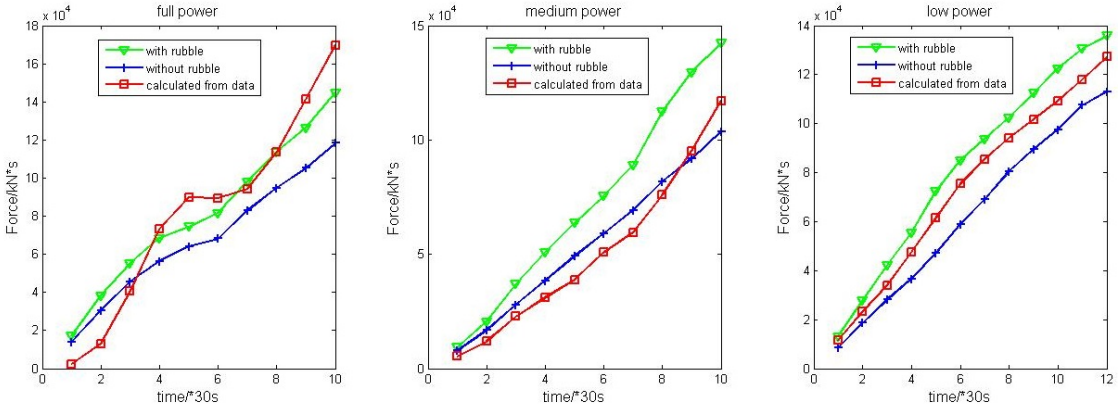

Figure 31: Time evolution of accumulative simulated resistance

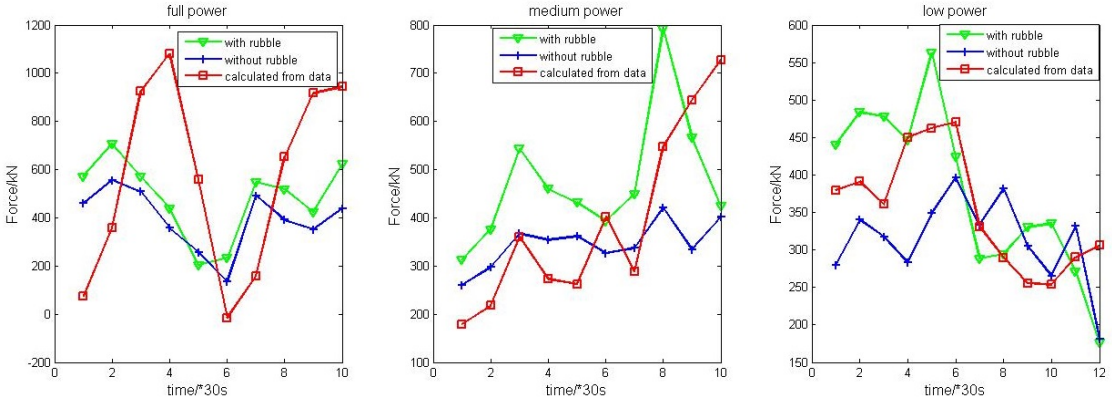

Figure 32: Time evolution of average simulated resistance within every half minute

are reduced to 4.32, 2.36 and 1.32 m/s, which gives 2%, -24% and -19% relative difference respectively.

Similarly, the time history of speed with non-linear pressure-area relationship implemented is plotted in figure 34, together with the results from random radius as reference. It is seen that non-linear relationship generally yields a higher velocity. The values and trends are again similar to those by model with only random radius. A closer result is seen with non-linear p-a relationship and rubble resistance under low power, as the bottom speed is about 0.9 m/s, just 0.2 m/s less than measured data. Average speeds with non-linear p-a are 4.96, 3.07 and 1.95 m/s while with rubble resistance they become 4.56, 2.34 and 1.45 m/s.

Time history of forces given with dynamic bearing capacity and non-linear p-a relationship are plotted in figure 35. Total ice resistance is plotted in dashed lines which includes ice sliding and submersion force in addition to ice crushing and breaking force. There is no obvious resistance change in terms of values or variations compared to the simulation results with only random breaking radius model. Total resistance is more than twice of ice breaking and crushing force, which indicates that the force due to underwater part takes up more than 50% of the

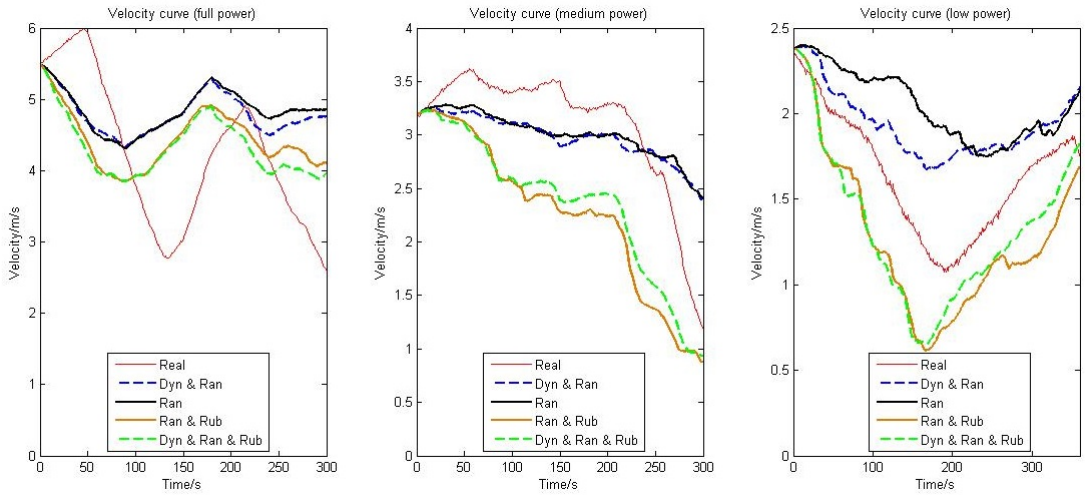

Figure 33: time history of speed with dynamic bearing capacity

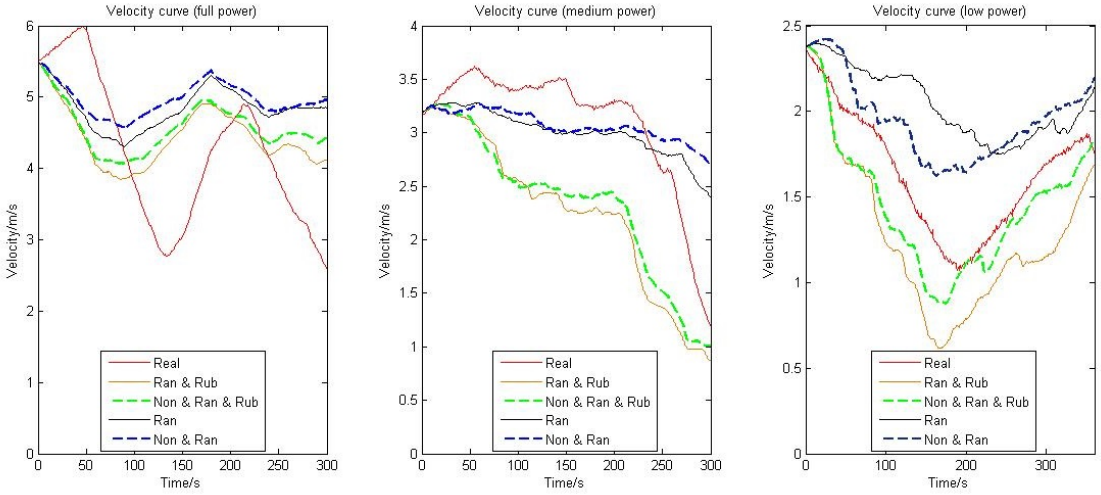

Figure 34: Time history of speed with non-linear p-a relationship

total resistance. Ice resistance due to rubble is not included here since it has been discussed in section 7.1.3. Ice resistance variation is generally consistent with the variation of ice thickness. For example with full power, ice thickness is very small from 150th to 180th second, which results in the smallest ice resistance during whole time period. Average resistance by dynamic bearing capacity and non-linear p-a under full, medium and low power case are 406, 350, 321 kN and 373, 328, 318 kN without rubble accounted. Compared to the results by the simulation only with random radius, dynamic bending tends to increase the resistance for all cases while non-linear model tends to decrease the resistance for full and medium power cases.

As a conclusion, with dynamic bending capacity or non-linear p-a, the shapes and values of the time history of speed do not change much. With rubble resistance included, there is again a significant reduction in speed values. The influence of

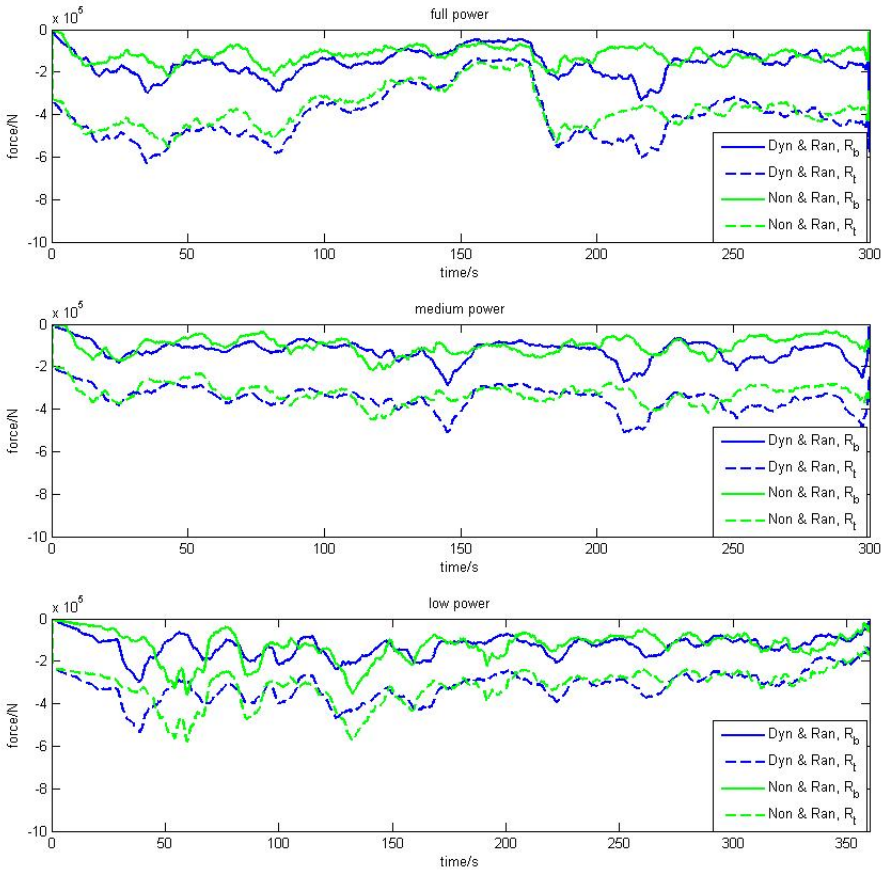

Figure 35: Time history of ice breaking (real line) and total (dashed line) resistance with dynamic bending (blue) and non-linear p-a (green)

dynamic bending and non-linear p-a on resistance values are quite limited.

7.1.5 Summary of numerical simulation results

A summary of average speed values are listed in table 8. Speeds given in the table are in m/s. The percentage values are the relative deviation compared to full scale data.

Table 8: Summary of velocity simulations

Model	$V_{full,ave}$	$V_{full,ave,rub}$	$V_{med,ave}$	$V_{med,ave,rub}$	$V_{low,ave}$	$V_{low,ave,rub}$
Real case	4.22	4.22	3.10	3.10	1.63	1.63
Ori	4.73(+12%)	-	2.76(-11%)	-	1.76(+9%)	-
Ran	4.84(+15%)	4.43(+5%)	3.01(-2%)	2.26(-27%)	2.05(+26%)	1.27(-22%)
Non & Ran	4.96(+18%)	4.56(+8%)	3.07(-1%)	2.34(-25%)	1.95(+20%)	1.45(-11%)
Dyn & Ran	4.79(+14%)	4.32(+2%)	2.99(-4%)	2.36(-24%)	1.93(+18%)	1.32(-19%)

Again, a summary of average resistance is made in table 9 for a better comparison of the results. It is shown that the resistance deviation is not as large as velocity deviation. By applying rubble resistance into the model, the prediction is improved by some extent.

Table 9: Summary of force simulations

Model	$R_{full,ave}$	$R_{full,ave,rub}$	$R_{med,ave}$	$R_{med,ave,rub}$	$R_{low,ave}$	$R_{low,ave,rub}$
Real case	567	567	391	391	355	355
Ori	395(-30%)	-	362(-7%)	-	343(-3%)	-
Ran	394(-30%)	483(-15%)	346(-12%)	475(+21%)	314(-12%)	378(+6%)
Non & Ran	373(-34%)	452(-20%)	328(-16%)	463(+18%)	318(-10%)	362(+2%)
Dyn & Ran	406(-28%)	504(-11%)	350(-10%)	465(+18%)	321(-10%)	370(+4%)

Since above tables only conclude the results from average view, information during the evolving process is hidden. Therefore, table 10 is made to list the findings and comments to the results and modifications.

Table 10: Findings and comments of simulation results

Model	Findings & Comments
Ori	Sudden change in speed and force, not realistic
Ran	Eliminate the sudden change, underestimate resistance when there is rubble accumulation, overestimate resistance during 0 to 210s with medium power but deviation is very small
Ran & Rub	Rubble resistance accounted, but overestimated
Dyn (& Rub)	No much changes in values or line trends, speeds slightly decrease with high speed and increase with low speed
Non (& Rub)	Speeds increase and resistance decrease, but not significant

7.1.6 Sensitivity study of C_l

For sensitivity discussion, simulation is run under medium power with C_l reset as 0.5 and 0.6. Time histories of speed from the simulation are plotted in figure 36, together with $C_l = 0.4$ for comparison. As illustrated, with a higher C_l, velocity is clearly increased. The final speed is increased from 0.9 m/s to 1.2 and then 1.4 m/s by altering C_l from 0.4, 0.5 to 0.6. The average resistance with C_l equal to 0.4, 0.5 and 0.6 are 475, 444 and 422 kN and average speed are 2.26, 2.51, 2.63 m/s.

Figure 37 makes boxplots of breaking radius under medium power with C_l equal to 0.4, 0.5 and 0.6. The median breaking radius varies from 1.7 m to 2.2 m and then 2.5 m with C_l increasing. There is also a larger scattering range when C_l increases.

7.2 Simulation results by empirical formulas

Simulated time histories of speed by Lindqvist's and Riska's formula are plotted in figure 38. As reference, real and numerically simulated time history of speed are also

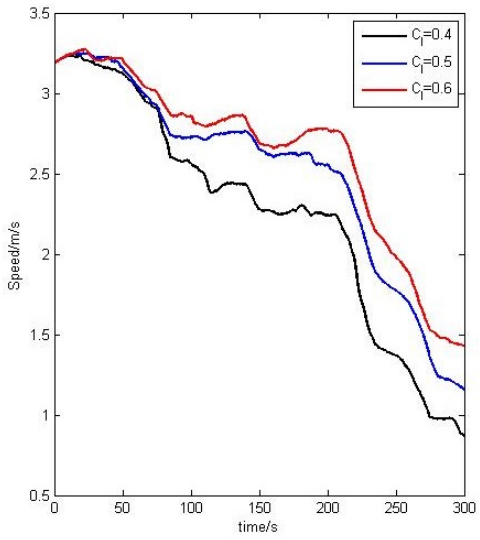

Figure 36: Time history of speed with C_l equal to 0.4, 0.5 and 0.6 under medium power, with random breaking radius and rubble resistance

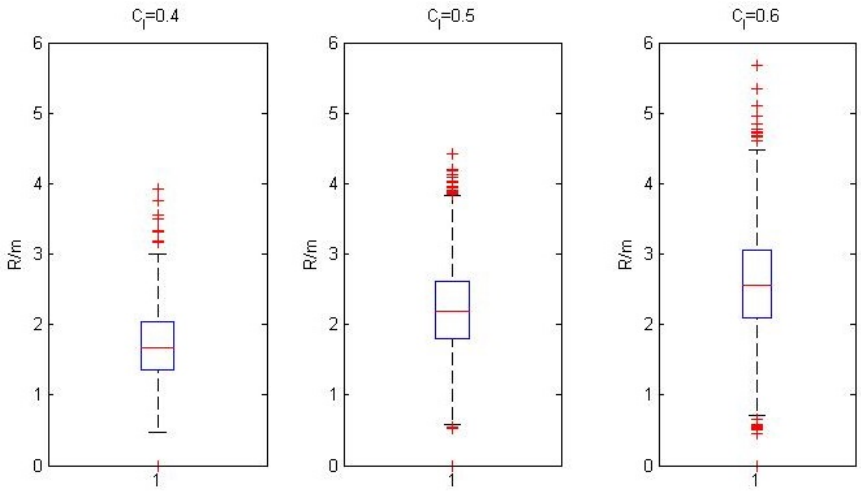

Figure 37: Boxplot of breaking radius with C_l equal to 0.4, 0.5 and 0.6 under medium power

plotted. These figures are drawn without rubble resistance included.

As drawn in the figure, Empirical formulas predict larger velocities than those given by numerical simulation. The curves by Lindgvist's formula generally follow similar varying trends with the real case, while those by Riska's just accelerate for most of the time. There are more significant difference with the real case by Riska's formula. One thing worth attention is that Lindqvist's method actually gives good predication in the first 3.5 minutes under medium power, while numerical simulation produces a little lower, but still good speed prediction.

Resistance curves are plotted in figure 39 and 40. Resistance curves by Lindqvist's

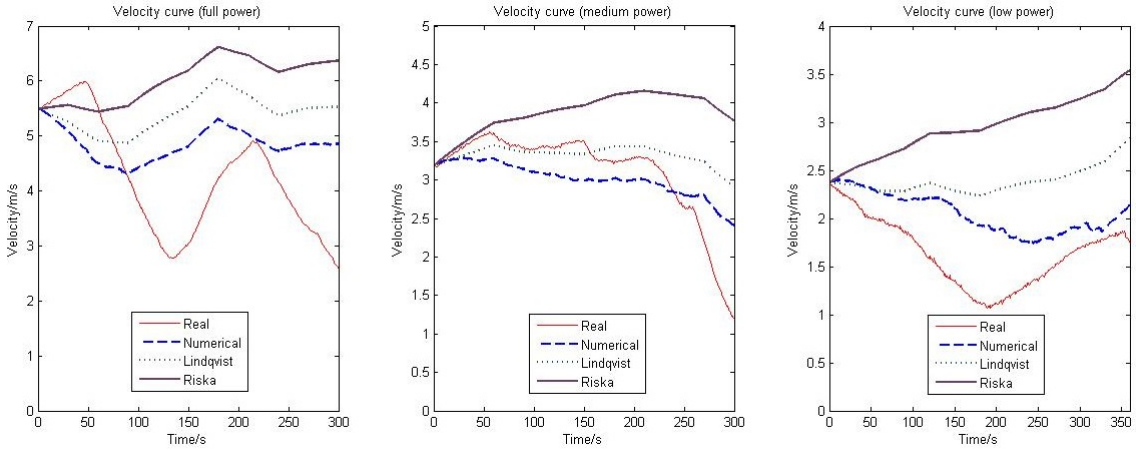

Figure 38: Time history of speed simulated by Lindqvist's and Riska's formulas

formula are divided into submersion force and ice breaking force. Resistance curves by Riska's formula are divided into parallel part resistance and bow part resistance. It shows that average resistance due to parallel ship part is around 50kN, which is smaller than predicted by numerical methods. A clear feature of these resistance curves is that they agree very well with ice thickness changes. This is same to numerical simulation results.

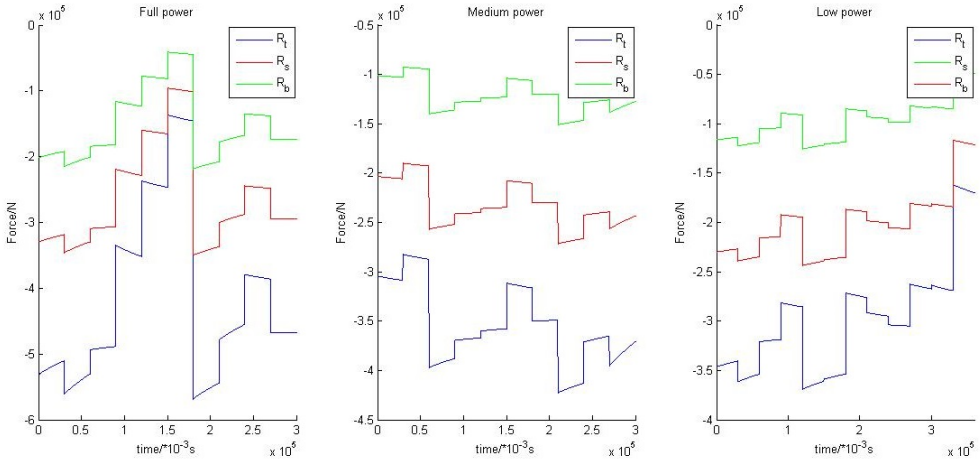

Figure 39: Time history of resistance by Lindqvist's formula

Table 11 is made to summarize a comparison between the results from numerical and empirical formulas. R_{ave} refers to the average resistance during whole test; V_{ave} is the average velocity and R_{par} is the resistance due to parallel ship part. It is seen that empirical formulas always predict a lower resistance and higher speed than those by numerical simulation. From the comparison of resistance due to shoulder part between numerical method and Riska's formula, numerical method gives a larger resistance due to parallel part. Resistance due to parallel ship part can takes up 20% of the total resistance according to numerical method.

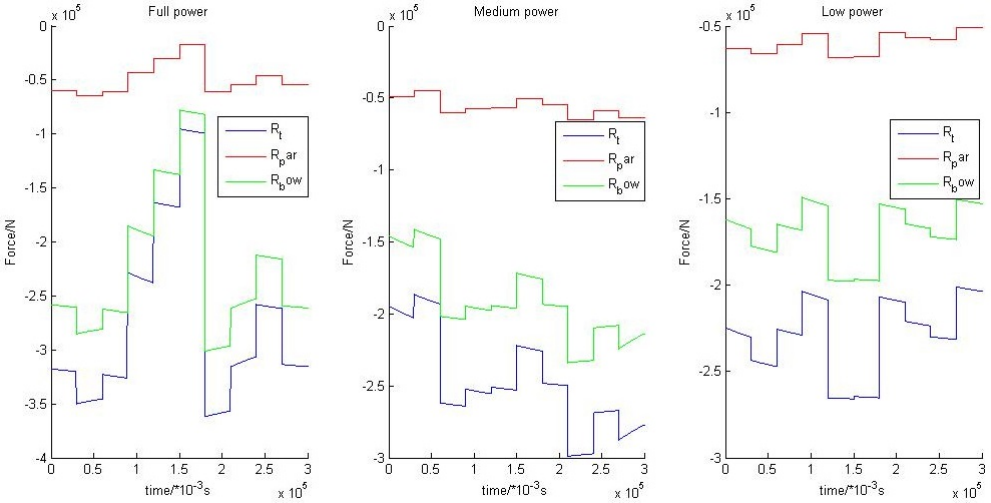

Figure 40: Time history of resistance by Riska's formula

Table 11: Comparison between numerical and empirical methods

Item		Real cases	Numerical	Lindqvist	Riska
Full power	R_{ave} (kN)	567	394	383	273
	V_{ave} (m/s)	4.22	4.84	5.40	6.02
	R_{par} (kN)	-	62	-	49
Medium power	R_{ave} (kN)	391	346	332	248
	V_{ave} (m/s)	3.10	3.01	3.33	3.88
	R_{par} (kN)	-	73	-	56
low power	R_{ave} (kN)	355	314	283	219
	V_{ave} (m/s)	1.63	2.05	2.38	2.95
	R_{par} (kN)	-	67	-	57

8 Discussions on simulation results

These informative results make it possible for a thorough discussion from different perspective. In this chapter, simulation is evaluated by comparison with full scale data and possible modifications and improvements are proposed and analysed. In section 8.1, an analysis is conducted on the reliability and usability of full scale data for evaluation use. Then built criteria in section 5.2 is used to compare the results with full scale data and empirical formulas in section 8.2 and 8.3. It is found that the model gives acceptable predictions and it has certain advantages over empirical formulas. The applied ridge formula is further discussed and analysed in section 8.4. In section 8.5, implemented modifications are discussed quantitatively. Ice breaking process has been theoretically examined in section 5.1. Simulation results will verify this analysis and tell how much effects the modifications have on prediction. Section 8.6 discussed shoulder crushing phenomenon which has a clear influence on the accuracy and usability of this model. Sensitivity of the model is shortly described in section 8.7 since it is not the main focus of this thesis. In the last section, possible error sources are looked into for a better understanding of the simulation.

8.1 Full scale data analysis

From data preliminary analysis in chapter 4 and simulation results in chapter 7, several points regarding full scale data are worth mentioning. Firstly, EM measured thickness data can be quite different from stereo camera measured data. The assumption that this difference is caused by ice rubble under level ice is well proved by simulation results, especially by medium and low power cases. In medium power scenario, ice rubble is only significant during last 1.5 minutes and with low power during first three minutes. During these time, speed from full scale data has a much steeper drop than simulation. From figure 32, simulated forces without rubble resistance are obviously smaller than reality during these time. This difference can be decently eliminated by implementing a ridge resistance formula to calculate rubble resistance. Therefore, resistance due to this rubble part should definitely be included in simulation. An interesting thing indicated by this is that although an ice field is visually identified as level ice as stated in Bekker et al. (2014), there still can be other ice parts like ice rubble beneath level ice, which can be detected by EM method instead but not stereo camera. The accumulation of ice rubble is very similar to ice ridge keel. There is a possibility that this visually identified level ice field is actually ice ridge field with low sail and keel. Since the measured ice rubble is mostly only 1 metre, the possible sail at the top of level ice could be no larger than 20 cm, which might be visually invisible if there is snow covering. This strongly supports a combined measurement of EM and stereo camera onboard a research icebreaker when doing full scale tests.

The second point comes from full power data. The calculated time history of resistance under full power in figure 15 is abnormal. Specifically, during 0s - 45s and 150s - 220s, calculated total resistance is around 100 kN. However, the resistance can be as much as 200 kN during 0s to 45s just considering submersion force. This

means that icebreaking force and rubble resistance are acting as propulsion, which is obviously not possible. As discussed in section 4.3, there is a possible phase difference around 30 seconds between ice thickness data and speed data. Since full power data has the most significant ice thickness variation (level ice from 0.1m to 0.3m), this 'phase difference' effect is much more obvious than the other scenarios with medium and low power. The assumption of phase difference is tested and well proved by the results when comparing calculated and simulated ice resistance. With the presence of this phase difference, there is no possibility to get a very similar time history of resistance to full scale data from simulation with full power data. Therefore, during following discussion, medium and low power simulation are the main sources to draw our conclusion while full power simulation is used just as a reference.

Since stereo camera data which is used to represent level ice does not change much during medium and low power tests, it is wise to divide the passage into segments, which makes the model easier to implement and clearer to tell something from results. Too small segments is unnecessary since ice thickness is actually randomly distributed in a certain area. For practical use, distance segments could be better because it reflects reality. However, since ice thickness and power data are synchronous in this full scale data, in this thesis, 30 seconds time segments for ice thickness and power data and 5 seconds segments for ice rubble thickness data are used while distance is simulated as an outcome. It performs well in terms of accuracy in prediction and proves that this method is proper for evaluation use.

8.2 Comparison with full scale data

As mentioned in section 5.2, resistance is most independent on previous resistance history, while time history of speed and average speed has accumulative effect. Therefore it is firstly discussed. Figure 32 and table 9 gives different perspectives to look into resistance from process view and average view. Obviously, from both views, resistance difference under full power is quite large, which differs from the other cases. As just discussed, full power data is used only as a reference. Looking into medium and low power cases, from average view, numerical model gives acceptable resistance prediction which is around 10% less than calculated resistance from full scale data without rubble resistance considered. When resistance due to ice rubble is included in total resistance, there tends to be an overestimation of resistance by an obvious extent. This indicates that the ridge resistance formula implemented here may give too large values of rubble resistance. According to figure 29, with 1.5 metres rubble thickness, the resistance can be as large as 600 kN, which is much larger than resistance from breaking level ice. From process view, the results strongly indicate that simulation without rubble considered fails to predict the resistance change at the time when there is apparent rubble accumulation. In a word, from resistance view, the simulation model is acceptable in predicting level ice. With rubble resistance considered, simulation results can better reflect the time variation of resistance, but seems to overestimate the results.

The time history of speed under all three power sets generally demonstrate some similarities to full scale data in line trends, but with clearly different values. Without

rubble resistance, simulated velocities are generally larger than real case, which means less resistance. The slope of the curves when velocity drops is not as significant as full scale velocities, especially when there is significant rubble accumulation. When ridge resistance formula is applied, the slope becomes larger than real, with a lower bottom speed in low power case. This gives similar conclusions as given by resistance comparison.

Average velocity difference under full power is not very large compared to full scale data (below 15%), while it is more obvious under low power (around 20%). One reason is that a same deviation takes up a larger percentage under low speed. Another reason is due to the accumulative effect stated in section 5.2. Ice rubble is influential during last 1.5 minutes for medium power and during first 3 minutes for low power. Therefore, the velocity deviation is more accumulated under low power, thus leading to a larger deviation. It can be misleading if focusing only on time history of speed and average velocity. Average velocity is greatly reduced by implementing a ridge resistance accounting for the resistance due to rubble under level ice. However, as shown in table 8, with rubble resistance, the average velocity under medium power gets far from reality. From figure 24 and 32, this difference is mainly caused by the overestimation of resistance during 0-3.5th minute, where there exists insignificant ice rubble accumulation but with too large predicted rubble resistance.

Since rubble thickness during first 3.5 minutes under medium power is not significant, this part could be used to look into the accuracy of the model for level ice resistance prediction. From figure 24 and 32, without rubble resistance considered, simulation tends to overestimate the resistance slightly. Average velocity within this period from full scale data is about 3.4 m/s while it is 3.1 m/s as simulated. Average resistance is 330kN by simulation, which is 15kN more than reality. The relative difference of resistance is around 5%, which is quite good. However, since there is still some rubble in this time period, the difference in prediction could be larger if resistance due to rubble is calculated accurately. This means that the model may overestimate level ice resistance slightly. But still, the prediction is acceptable.

As a conclusion of the evaluation, it would be decent to say the simulation generally gives an acceptable results in terms of level ice resistance and velocity. However, resistance due to ice rubble is overestimated. This needs improving for better prediction.

8.3 Comparison with empirical formulas

The results have illustrated a lower resistance with higher velocity in prediction by both Lindqvist's and Riska's formulas. Resistance deviations are quite large by empirical methods (around 20% less by Lindqvist's formula and 30% less by Riska's formula). Time history of speed by Lindqvist's formula locate above those by numerical methods in the figures. However, since ice rubble resistance is not included in these formulas, there is the possibility that the prediction by empirical formulas could be improved after considering ice rubble. Actually, as shown in figure 38, the prediction is seen better by Lindqvist's formula during first 3.5 minutes under

medium power. Since rubble resistance is small during this time period, level ice resistance of reality may be closer to the values by Lindqvist's formula rather than simulation. However, due to possible error sources, the conclusion can not be drawn for sure since the deviation of resistance by numerical simulation is just 5% within this 3.5 minutes. With Riska's formula, time history of speed performs very strange since resistance is too low. The real resistance of this modelled ship induced by level ice is very likely to be close to the predictions by numerical simulation and Lindqvist's formula, which are beyond that by Riska's formula. The average velocity by empirical formulas is also larger than that by numerical simulation. However, according to Kuuliala (2015), the resistance of MT Uikku given by numerical simulation lies between those given by Lindqvist's and Riska's formula. This difference is noticed here and discussed as a reference to look into the performance of these methods.

It is clear that compared to numerical simulation, empirical formulas does not take many details of ship dimensions into calculation. Only ship main dimensions and several angles at certain position are considered in the formulas. Numerical method models the ship waterline together with the angles around the line. It detects every contact between ship and ice and then sum up all the contact forces together. MT Uikku is a tanker with 81° slope along parallel ship area. This make it possible to break ice with a sway or yaw motion. Thus friction force due to crushing is less significant compared to S.A. Agulhas, which has a long vertical parallel ship hull. When the ship is creating a narrow channel, S.A. Agulhas is more exposed to friction force during the contact with the ice. This difference is beyond the scope of empirical formulas, which in this case, possibly underestimate the force due to parallel ship part. This can be partly deduced from table 11, where Riska's formula gives a smaller value of parallel resistance. Thus it is reasonable to say that numerical method has an advantage in predicting ship resistance for a specific case.

However, it should still be kept in mind that the numerical simulation method is still greatly relied on empirical formulas. Submersion and rubble forces are calculated according to Lindqvist's formula. From the force components shown in figure 4, submersion force takes up more than 50% of total ice forces, which is a huge part. It is necessary to investigate the deviation due to submersion force in future work.

8.4 Rubble resistance

As discussed in section 8.1, the difference in measured ice thickness strongly indicates that there is ice rubble accumulation under level ice. These ice rubble are likely to be ridge keel. Therefore, a ridge resistance formula from Riska et al. (1997) based on Malmberg (1983) is implemented into the simulation to take rubble resistance into account.

Simulation results have proved the effectiveness of taking rubble into account. It gives a more similar time evolution of resistance to those from full scale data, as shown in figure 32. However, there is a clear overestimation of resistance by implemented ridge resistance formula. This is possibly partly due to the inclusion of snow in measured rubble thickness. Another reason is that with small rubble thickness, such as 1 metre, the assumption in the derivation of this ridge resistance is

not well met. The calculation of the bow resistance due to ridge keel in the formula shown by equation 36 assumes that the rubble is accumulated in front of ship bow along the whole depth. However, for the data used in this thesis, ship depth is much larger than rubble thickness. It is not very likely that the rubble could cover the whole ship depth. This will lead to an overestimation of resistance, which is consistent with the simulated results in this thesis. In addition, another deficiency of this ridge resistance formula is that it does not take ship speed into account. The formula is derived for a ship with slow motion. In this thesis, with full power, the velocity can be 5 m/s, which is far from static. Assuming the resistance due to rubble will increase with speed growing, the lack of resistance by simulation can be explained by speed effect.

8.5 Analysis of the modifications

p-a relationship The time history of speed in figure 34 and force summary in table 9 indicates that the non-linear p-a relationship model implemented in this thesis usually reduce the predicted resistance by around 5%. This is consistent with the discussion in section 5.1. This modification does not have a great influence on the time history of speed as shown in figure 24. It only increases speed values slightly. There is no clear advantage seen in prediction with non-linear pressure-area implemented.

However, it does not necessarily mean that a non-linear p-a relationship is meaningless. A different loading rate could give quite different resistance values according to section 5.1. Tan et al. (2013) stated that the ship speeds after considering his p-a relationship are lower than before. Therefore, a reasonable loading rate could make the prediction closer to real case. Literatures on pressure-area relationship give quite diverse conclusions. As shown in table 1, researchers generally agree on an expression in the form of CA^{α}, but with different values of C and α. Moreover, according to Daley (2007), p-a relationship should be divided into spatial and process pressure distribution, which is obviously not considered when the p-a formulas in table 1 were derived. In a word, the research up to now is far not enough to decently describe the loading process. Therefore, it is not necessary to implement this model before a more convincing theory is proposed.

Area modification Area modification is discussed here immediately after p-a relationship because they are both concerning loading rates. Although it is not implemented in this thesis due to computational reasons, it could still give a clue that this area modification will produce larger resistance for prediction, as it slows down the loading rate. The original point of this modification is that the ice sheet will be suppressed by the ship when contacting, thus reducing the contact area. This is obviously true in reality. So this modification is likely to produce positive results and thus should be applied. However, it should be smartly implemented, in a way that is less expensive for computation. Unfortunately, the author has not got enough time to do this so the discussion of area modification has to stay at this level.

As an extension, it is interesting to have a look at different types of areas shown in figure 41. This figure demonstrates that the detected contact area, which is referred to as nominal area here, is larger than than true area. This tells that the contact area detected in simulation may be overestimated.

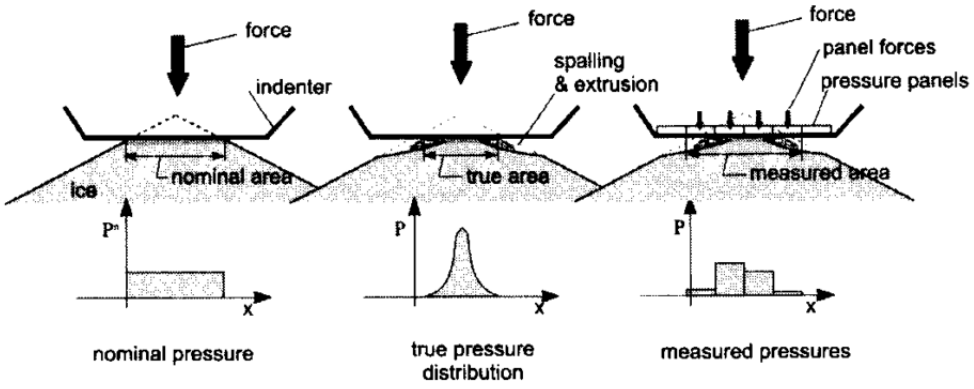

Figure 41: Types of areas (Daley 2007)

Dynamic bending According to the results, dynamic bending model increase the total resistance under full power case and reduce under medium and low power. According to figure 6.3, bearing capacity are increased when a relative velocity normal to contact plane is above 0.312 m/s and reduced below that value. With low power and velocity, bearing capacity is more likely to reduce, leading to smaller resistance. This proves that the simulation becomes more dynamic with velocity change when applying dynamic bearing capacity model. In addition, from the expression of P_f in equation 24, the simulation also becomes more sensitive on thickness change at a relatively larger velocity. Since the results does not seems to be very dynamic at high speed, this modification actually helps to improve this. However, it should be noticed that this improvement is very slight according to figure 33. Time history of speed does not change much with this model implemented. The best benefit of this model is that it helps it get rid of an empirical coefficient C_f, which is a good point for numerical simulation. With dynamic bearing capacity, it is not required to manually select a C_f any more.

Random radius As aforementioned in chapter 7, an obvious advantage of implementing random breaking radius is that it reduces the strong fluctuation in the output with original model. Random breaking radius controls shoulder crushing within a smooth and regular behaviour and avoid sudden change in crushing force and velocity. Su et al. (2014) also pointed that when a random breaking radius is applied the simulation results are more smoothly distributed along the fitted regression line in h-v curve. This is a great advantage when the model is used in design to predict ship performance with no real data as reference. Moreover, a random breaking radius reflects more about reality. There are many randomness existing in ice characters

like crushing strength and thickness, all of which lead to a randomly distributed ice breaking radius. Therefore, it should definitely be applied into original model.

However, it should also be kept in mind that the distribution applied for breaking radius is not based on model test or full scale measurement. Su et al. (2014) also argued that a lognormal distribution may reflect the real case better. Since the distribution of breaking radius is influential to predicted ice breaking resistance, a more realistic distribution of breaking radius could also help to better predict the resistance.

8.6 Shoulder crushing

As mentioned in chapter 7, shoulder crushing can obviously be seen without random breaking radius model. This phenomenon could result in a sudden drop in velocity, leading to a velocity deviation afterwards. Su et al. (2014) stated that with random breaking radius, intermittent shoulder crushing occurs instead of consistent shoulder crushing. From table 9, with random breaking radius, average resistance actually does not change much. So the main influence is on time history of speed. Since the seriousness of shoulder crushing can be affected by the standard deviation of radius distribution, it is necessary to know how shoulder crushing acts in reality, in order to check if it has been overestimated or underestimated.

Shoulder crushing also reflects the influence of sway and yaw motion on simulation. The model simulate planar motions. Since the friction force occurs due to the crushing force in y-axis, it only happens when there is sway or yaw motion. This shows the advantage of introducing other degrees of freedom into the model. As motions consumes energy, it is possible to produce a result with smaller average velocity if other degrees (pitch, heave and roll) are also considered.

8.7 Sensitivity of the model

The sensitivity problem of the model is discussed in the master thesis of Kuuliala (2015), where the three implemented empirical coefficients C_l, C_v and C_f are investigated. The conclusion is that resistance is not very sensitive to these empirical coefficients in thin ice around 0.4m. However, since C_l value used in this thesis is out of the tested range in Kuuliala's thesis (0.8-1.1), in this thesis, one test regarding sensitivity on C_l with a range of 0.4 to 0.6 is conducted with medium power. From the qualitative analysis in section 5.1, C_l is crucial in determining breaking radius, which determines how long an icebreaking period can be. The results presented in figure 8.7 tells that the model can be very sensitive on C_l in the range of 0.4 to 0.6. Average resistance could have an difference of 53kN when C_l is changed from 0.4 to 0.6. Thus it is very important to find a suitable value for C_l. Since these coefficients could only be measured by model test or full scale test, it is not possible to justify which sets of coefficients is correct only by this simulation. For S.A. Agulhas II, a combination of (0.4, -0.12, 3.2) for C_l, C_v and C_f seems to give an acceptable prediction. As discussed in section 8.2, the simulation may underestimate

level ice resistance slightly. Therefore, C_l is suggested to be between 0.4 to 0.5 for S.A. Agulhas II.

8.8 Discussion on error sources

There are a couple of error sources which hinders this thesis for a more convincing conclusion. It can be the thickness measurements, net thrust model, hydrodynamic forces or the simulation itself. A discussion on error sources could give a better vision on the results and conclusions.

Figure 15 is a good example to give an image of where the errors can came from. As already discussed in section 8.1, there is possibly a phase difference between ice thickness and time history of speed. This makes full scale data inappropriate for evaluation use in this thesis and also introduces slight deviation into medium and low power simulation.

The error could also come from net thrust model and power-speed dependence assumption. Since these are derived from regression methods according to data of many ships, it could have some deviation for a specific ship. If these data can be given by model test or full scale test, this error source could be eliminated.

Resistance due to ice rubble under level ice could be another error source. The large difference in EM and stereo camera measured thickness demonstrates the existence of another resistance source. Since the measurement did not give information on what this difference is composed of, although this part have been calculated in the simulation by a ridge resistance formula, it is still very likely that the calculation overestimates the resistance. The data is likely to include a certain thickness of snow, which will not cause as much resistance as rubble does. The simulation is possible to be improved if snow thickness is subtracted from rubble and if this formula is modified to better calculate resistance due to ice rubble around 1 metre.

Another error source is the simulation itself. Due to coding reasons, the model is further simplified on crushing. Ice along bow part is not crushed away, which means that crushing force from the same ice area can act on the ship again if it has not experienced a bending failure. This crushing is done among parallel ship area because the ship hull is vertical, making this change much easier to implement. The author has tested the effect of this change and found that without ice crushing away along parallel part, the sway and yaw forces and motions can be very large, which greatly affects the results. This influence is reduced mostly by crushing away the ice along parallel ship part. But still there can be small effect on simulation results.

The way that power and level ice thickness data are averaged every 30 seconds will also make some difference from reality. However, as shown in figure 12 and 13, ice thickness and power does not change much during medium power (first 3.5 minutes) and low power scenarios. Therefore, this average method could not lead to significant deviation.

9 Conclusions, recommendations and future work

The aims of this thesis listed in section 1.2 are achieved. Full scale test gives different ice thickness by EM and stereo camera measurements. Stereo camera measured data can be used as level ice thickness. The added part which is derived by subtracting stereo measured thickness from EM measured thickness can be regarded as ice rubble, which also contributes to resistance. Ridge resistance formula can be applied for the calculation of resistance due to these rubble. The results show that this is necessary to be counted into total resistance but it tends to overestimate the resistance. The formula needs to be improved to better predict rubble resistance when the thickness is small. The combined measurement method using both EM device and stereo camera is highly recommended for future sea trial due to its capability to give comprehensive information of ice and tell more facts beyond visual observation. A visually observed level ice field may have ice rubble beneath the consolidated layer, which acts like ridge keel. Beside thickness data, full power data concerning power and velocity seems strange when looking at real resistance. The reason could be a phase difference of around 30 seconds between ice thickness and speed data due to the installed position of measurement device. This should be noticed when these data are used in future research.

By comparing the simulation results with full scale data, this semi-empirical numerical simulation method proves to be acceptable in predicting continuous ship motion under changing power sets and ice parameters, with a deviation generally below 20% both for average resistance and velocity. Time history of speed generally shows similar trends to reality but with different values. The simulation is likely to overestimate level ice resistance slightly. So a larger C_l between 0.4 and 0.5 is recommended for S.A. Agulhas II. The deviation in terms of velocity and resistance is not large and not divergent so it can be concluded that this method is capable to predict ship resistance and motions under changing environment for long period simulation.

Comparing with empirical formulas, numerical method proves its advantage in presenting more ship-specific results. Since it takes detailed ship diameters into consideration, numerical simulation can give quite different results for ships with similar overall dimensions. Besides, numerical simulation also predicts ship motions in sway and yaw, which is coupled with force in surge direction by friction force. Sway and yaw motions are highly relevant to shoulder crushing, which is identified to be an influential phenomenon during simulation. In a word, numerical could give more accurate predictions than empirical formulas which actually represents an average performance of different ships. However, it should also be noticed that the method is still semi-empirical, which relies on empirical formulas in a large extent. Efficient numerical methods concerning submersion resistance and ridge resistance are required for further developing the simulation.

Pressure-area relationship and area modification affect the outcome by altering the loading rate. Both are important points for an accurate prediction but still requires some work before they can be effectively implemented. Due to the complexity in ice crushing mechanism, it is inevitable to include the deviation due to p-a relationship.

As an recommendation, model test or full scale test should be conducted particularly on 'process p-a relationship', instead of spatial p-a relationship, which are mostly mixed together during the derivation of current p-a relationships. Factors influential to the relationship like temperature or salinity should be controlled in order to get a convincing conclusion. Area modification should also be checked by tests and then implemented in a smarter way. It is suggested by the author that at current stage, linear p-a relationship should be kept before a more convincing theory is proposed while area modification should be applied in an efficient way.

Random breaking radius well controls the uncertainty in the outcome of the model by reducing the possibility of serious shoulder crushing. The time history of speed behaves much more regular with random breaking radius. This improves the model by imitating the reality. For this reason, it should be definitely implemented into simulation. However, this modification will change the resistance value inevitably since it changes the length of an ice breaking period. As the distribution of breaking radius is not based on measurements, the justification of this normal distribution is doubtful. A better distribution from model or full scale test may reflect the reality better and thus improves the results of prediction.

Dynamic bearing capacity model introduces more dynamic features into this model. Resistance dependency on velocity and ice thickness are increased. The results show slight increase on dynamic features but do not change resistance values much. The main advantage of this model is that it helps to overcome an empirical coefficient which is decided manually. This is very good for simulation. So the recommendation regarding modifications is to apply random breaking radius, dynamic bending capacity and area modification at current stage, but ignore non-linear p-a relationship before a mature theory comes into use.

As aforementioned, the model is quite sensitive on C_l. Since C_l is an important factor determining ice breaking radius, it is strongly suggested to conduct relevant tests regarding broken floe size. Ice breaking pattern is an crucial part in the accuracy of prediction. A progress in the determination of broken ice floe size would improve this simulation method onto a new level. Unfortunately, the author is not able to come up with a better way for the determination of breaking radius. Before an improvement is achieved, the author suggest C_l to be between 0.4 and 0.5 in order to give a decent prediction.

For future work, stress should be put on following things. First and most importantly, model or full scale tests should be conducted on a more deterministic relationship (instead of empirical coefficients) between floe size and ship velocity as well as ice thickness. At early stage, the shape of broken ice floe can be neglected since the size matters more. Secondly, a modified version of ridge resistance formula is required to calculate rubble resistance when it is thin compared to ship depth. Besides, there are some possible work which could improve the simulation accuracy but are not urgently needed. Studies could focus on the crushing process which aims at a more accurate loading rate. In addition, the distribution of broken ice floe size could be investigated. Moreover, since this method is still highly relied on empirical formulas, there is still some way to go before the whole ice breaking process can be numerically simulated.

References

[1] Aksnes, V. A simplified interaction model for moored ships in level ice. *Cold Regions Science and Technology,* 2010, 63(1-2), 29–39.

[2] Aksnes, V. A panel method for modelling level ice actions on moored ships. Part 1: Local ice force formulation. *Cold Regions Science and Technology,* 2011a, 65(2), 128–136.

[3] Aksnes, V. A panel method for modelling level ice actions on moored ships. Part 2: Simulations. *Cold Regions Science and Technology,* 2011b, 65(2), 137–144.

[4] Bekker, A., Suominen, M., Peltokorpi, O., Kulovesi, J., Kujala, P., & Karhunen, J. Full-scale measurements on a polar supply and research vessel during maneuver tests in an ice field in the Baltic sea. *Proceedings of the 33rd International Conference on Ocean, Offshore and Arctic Engineering* 2014.

[5] Berglund, T. Ice fracture model for real-time ship simulator. Master's Thesis, Norwegian University of Science and Technology, Trondheim, 2012.

[6] Daley, C. Reanalysis of ice pressure-area relationships. *Marine Technology,* 2007, 44(4), 234-244.

[7] Das, J.,& Ehlers, S. Numerical simulation of crushing and bending failure of ice using SPH. *Proceedings of the ASME 2015 34th International Conference on Ocean, Offshore and Arctic Engineering,* 2015, pp. 1–8

[8] Enkvist, E. *On the ice resistance encountered by ships operation in the continuous mode of ice breaking.* Report 24. The Swedish Academy of Engineering Sciences in Finland, 1972.

[9] Izumiyama, K., Kitagawa, H., Koyama, K., & Uto, S. A numerical simulation of ice-cone interaction. *Proceedings of the 11th IAHR International Symposium on Ice,* 1992, Banff, Alberta.

[10] Jones, S.J. Ship in ice - a review. *25th Symposium on Naval Hydrodynamics,* August 2004, St. John's, Newfoundland and Labrador, Canada.

[11] Kotovirta, V., Jalonen, R., Axell, L., Riska, K., Berglund, R. A system for route optimization in ice-covered waters. *Cold Regions Science and Technology,* 2009, 55(1), 52–62.

[12] Kovacs, A., & Morey, R. M. Sounding sea ice thickness using a portable electromagnetic induction instrument. *Geophysics,* 1991, Vol. 56, NO. 12.

[13] Kulovesi, J & Lehtiranta, J. Level ice thickness measurement using ship-based semi-automatic computer vision. *Proceedings of the 22nd IAHR International Symposium on Ice,* 2014, 679-686.

[14] Kuuliala, L. Feasibility study of a semi-empirical simulation model for level ice breaking. Master's Thesis, Helsinki University of Technology, Espoo, 2015.

[15] Lau, M. *Discrete element modeling of ship manoeuvering in ice.* Tech. rep. Research council of Canada, 2006.

[16] Lensu, M., Kujala, P., Kulovesi, J., Lehtiranta, J., & Suominen, M. Measurements of Antarctic Sea Ice Thickness during the Ice Transit of S.A. Agulhas II. *Proceedings of the 23rd International Conference, Port and Ocean Engineering Under Arctic Conditions,* 2015.

[17] Lindqvist, G. A straightforward method for calculation of ice resistance of ships. *Proceedings 10th International Conference, Port and Ocean Engineering Under Arctic Conditions,* 1989, Vol. 2. Luleä, pp. 722-735.

[18] Liu, J.C., Lau, M. and Williams, F.M. Mathematical modeling of ice-hull interaction for ship maneuvering in ice simulations. *Proceedings of 7th International Conference and Exhibition on Performance of Ships and Structures in Ice (ICETECH),* 2006, Banff, Alberta, Canada.

[19] Lubbad, R., & Løset, S. A numerical model for real-time simulation of ship-ice interaction. *Cold Regions Science and Technology,* 2011, 65(2), 111-127.

[20] Malmberg, S. On the mechanism of getting stuck in ice. M.sc. thesis, Helsinki University of Technology, Espoo, 1983.

[21] Masterson, D. M., Wright, B., Karna, T., & Maddock, W. P. A revised Ice Pressure-Area Curve. *Proceedings of 18th International Conference, Port and Ocean Engineering Under Arctic Conditions,* 2007, Dalian, China, 305-314.

[22] Matusiak, J. "Ship Dynamics", 2013.

[23] Newmark, N. A method of computation for structural dynamics. *Proceedings of the American Society of Civil Engineers,* 1959, Vol. 85. 3, pp 67-94.

[24] Palmer, A. C., Dempsey, J. P., & Masterson, D. M. A Revised ice pressure-area curve and a fracture mechanics explanation. *Cold Regions Science and Technology,* 2008, 56(2-3), 73-76.

[25] Riska, K., Wilhelmson, M., Englund, K., and Leiviskä, T. *Performance of merchant vessels in ice in the Baltic.* Research Report 52. Helsinki: Winter Navigation Research Board, 1997.

[26] Sanderson, T. J. O. *Ice Mechanics-Risks to Offshore Structures,* Graham and Trotman, London, UK, 1988.

[27] Sawamura, J. & Tachibana, T. Development of a numerical simulation method for rotatiog and sliding of the ice floes along a ship hull. *Proceedings of the 21st International Conference on Port and Ocean Engineering Under Arctic Conditions,* 2011

[28] Sawamura, J. Riska, K., and Moan, T. Numerical simulation of breaking patterns in level ice at ship's bow. *Proceedings of the 19th International Offshore and Polar Engineering Conference,* Osaka, Japan, 2009, pp. 600-607

[29] Su, B. Numerical predictions of global and local ice loads on ships. Phd thesis, Norwegian University of Science and Technology, Trondheim, 2011.

[30] Su, B., Roger, S., Tor, E. B. Numerical assessment of a double-acting offshore vessel's performance in level ice with experimental comparison. *Cold Regions Science and Technology,* 2014, 35(4), 317-332.

[31] Suominen, M., Karhunen, J., Bekker, A., Kujala, P., Elo, M., von Bock und Polach, R., Håkan, E, Saarinen, S. Full-Scale Measurements on Board Psrv S.a. Agulhas Ii in the Baltic Sea. *Proceedings of the 22nd International Conference on Port and Ocean Engineering Under Arctic Conditions,* 2013

[32] Suominen, M., Kulovesi, J., Lensu, M., Lehtiranta, J., and Kujala, P. A comparison of Shipborne Methods for Ice Thickness Determination. *22nd IAHR International Symposium on Ice,* Singapore, August 2014.

[33] Tan, X., Su, B., Riska, K., & Moan, T. A six-degrees-of-freedom numerical model for level ice-ship interaction. *Cold Regions Science and Technology,* 2013, 92, 1-16.

[34] Tan, X., Riska, K., & Moan, T. Effect of dynamic bending of level ice on ship's continuous-mode icebreaking. *Cold Regions Science and Technology,* 2014, 106-107, 82-95.

[35] Timco, G. W., & Weeks, W. F. A review of the engineering properties of sea ice. *Cold Regions Science and Technology,* 2010, 60, 107-129.

[36] Timco, G. W., & Sudom, D. Revisiting the Sanderson pressure–area curve: Defining parameters that influence ice pressure. *Cold Regions Science and Technology,* 2013, 95, 53-66.

[37] Valanto, P. The resistance of ship in level ice. *SNAME Transactions,* 2001, Vol. 109, pp. 53-83.

[38] Wang, S. A dynamic model for breaking pattern of level ice conical structures. Phd thesis, Helsinki University of Technology, Espoo, 2001.

[39] Zhou, L. Numerical and experimental investigation of stationkeeping in level ice. Phd thesis, Norwegian University of Science and Technology, Trondheim, 2012.

[40] Zhou, Q., Peng, H., & Qiu, W. Investigations of ship – ice interaction and maneuvering performance in level ice. *Cold Regions Science and Technology,* 2016, 122, 36-49.